

Many-Body Invariants for Multipoles in Higher-Order Topological Insulators

Byungmin Kang,¹ Ken Shiozaki,² and Gil Young Cho^{3,*}

¹*School of Physics, Korea Institute for Advanced Study, Seoul 02455, Korea*

²*Yukawa Institute for Theoretical Physics, Kyoto University, Kyoto 606-8502, Japan*

³*Department of Physics, Pohang University of Science and Technology (POSTECH), Pohang 37673, Republic of Korea*

(Dated: December 15, 2024)

We propose many-body invariants for multipoles in higher-order topological insulators by generalizing Resta's pioneering work on polarization. The many-body invariants are designed to measure multipolar charge distribution in a crystalline unit cell, and they match the localized corner charge originating from the multipoles. We provide analytic arguments and numerical proof for the invariants. Furthermore, we show that the many-body invariants faithfully measure the physical multipole moments even in the regime where the symmetries quantizing multipoles are lost and thus the nested Wilson loop indices cannot be applied.

Theory of macroscopic polarization in a crystal lies at the heart of the modern development of topological band insulators.¹ The theory provides a classic example of how the non-trivial topology of bulk ground states can determine the quintessential properties of the quantum phases such as symmetry-enforced boundary states.^{2,3} Furthermore, it nicely illustrates how the associated topology can and cannot be diagnosed; the topology cannot be measured by a local operator, but only through a gauge-invariant number defined in momentum space referred as the Zak phase,⁴ or through a non-local many-body invariant.⁵ In particular, the discovery of the many-body invariants for various topological insulators drastically increased our understanding of topological states and expanded the range of the search for the topological states beyond free-fermion limits, e.g., strongly-correlated systems and bosonic models.^{6–10}

Recently, a new class of topological states, namely higher-order topological insulators, has been discovered.^{11–19} Interestingly, these higher-order states are constructed out of the electric multipoles, which materialize as topologically-protected modes at the corners and hinges of the physical boundary. To characterize such higher-order topology, the so-called “nested Wilson loop” approach¹² has been put forward and used to detect the quantized multipoles. However, the nested Wilson loop indices successfully work only when there exist symmetries which quantize the multipole moments¹² and currently there is no generic bulk measure for the multipoles working even in the absence of the symmetries. Also, a new class of higher-order topological insulator has been introduced under the name an anomalous topological insulator¹⁹ whose non-trivial multipole moments cannot be diagnosed by a naive application of the nested Wilson loop approach. Moreover, the nested Wilson loop is genuinely a free-fermion quantity and thus cannot be a generic diagnosis for the higher-order topology in a general many-body condensed matter system. This opens a question how to define multipoles going beyond the nested Wilson loop picture and hence the associated higher-order topology in a condensed matter system.

In this Letter, we propose a set of many-body invari-

ants for the multipoles in crystalline systems, which successfully measure the multipole moments even when the quantizing symmetries are lost so that the nested Wilson loop indices can be used to detect the true bulk moments. In stark contrast to the nested Wilson loop approaches, we utilize real-space charge distribution, which can be evaluated even for strongly-correlated systems. To this end, we extend Resta's general definition of polarization⁵ to the multipoles:

$$P_x = \frac{1}{2\pi} \text{Im} \left[\log \langle \hat{U}_1 \rangle \right], \quad \hat{U}_1 = e^{2\pi i \sum_x \hat{p}_x}, \quad (1)$$

where $\hat{p}_x = \frac{x\hat{n}(x)}{L_x}$ is the polarization density (relative to $x = 0$) in the system of the length L_x with $\hat{n}(x)$ being the electron number at site x , and the sum is running over the whole system. Here the expectation value $\langle \hat{U}_1 \rangle$ is over the many-body ground state subject to the periodic boundary condition, i.e., $x \sim x + L_x$. Compared to the Berry-phase expression⁴ defined in momentum space, the above formula Eq. (1) provides a clearer picture of the macroscopic polarization P_x by relating it to the local microscopic polarization density \hat{p}_x . It also has played an important role in developing theories of related topological states^{20,21} and other strongly-correlated systems, which is known as generalized Hastings-Oshikawa-Lieb-Schultz-Mattis theorem.^{22–24}

Here, we define the macroscopic quadrupole moment in a crystal as following:

$$Q_{xy} = \frac{1}{2\pi} \text{Im} \left[\log \langle \hat{U}_2 \rangle \right], \quad \hat{U}_2 = e^{2\pi i \sum_{\mathbf{r}} \hat{q}_{xy}(\mathbf{r})}. \quad (2)$$

Here $\hat{q}_{xy} = \frac{xy}{L_x L_y} \hat{n}(\mathbf{r})$ is the quadrupole moment density (relative to $x = y = 0$) per unit cell at the site \mathbf{r} . Similar to Eq. (1), L_x and L_y are the sizes of the system. Analogously, the macroscopic octupole moment is defined as:

$$O_{xyz} = \frac{1}{2\pi} \text{Im} \left[\log \langle \hat{U}_3 \rangle \right], \quad \hat{U}_3 = e^{2\pi i \sum_{\mathbf{r}} \hat{o}_{xyz}(\mathbf{r})}. \quad (3)$$

Here $\hat{o}_{xyz} = \frac{xyz}{L_x L_y L_z} \hat{n}(\mathbf{r})$ is the octupole moment density per unit cell; the generalizations to higher-order poles follows immediately. As in Resta's formula, we use a

many-body ground state defined on the torus with periodic boundary conditions and each multipole moment density is summed over the whole space. Our real-space invariants provide a complementary view to the momentum space approach, the nested Wilson loop indices.¹² Below, we will explain the physics hidden behind these expressions and provide generalized formula, including a variation of Resta's foundational work Eq. (1).

A few remarks are in order. First, the multipole moments defined as above are ambiguous up to “mod 1” because of the periodicity of complex phases; this ambiguity reproduces the observation made in the previous studies.^{11,12} Second, we emphasize that the above expressions are truly many-body invariants because, when the exponentials are expanded, they require to measure $\sim \sum_{\mathbf{r}_1, \mathbf{r}_2, \dots, \mathbf{r}_J} \langle \hat{n}(\mathbf{r}_1) \hat{n}(\mathbf{r}_2) \cdots \hat{n}(\mathbf{r}_J) \rangle$, and this does not reduce to the product of the few-particle observables. To evaluate Eq. (2) and Eq. (3), we need the full knowledge of the many-body ground state. On the other hand, the expressions are gauge-invariant, i.e., it is independent of the basis choice, and thus they measure physical quantities.

We can also show that the expressions Eq. (2) and Eq. (3) are invariant under the superposition of the trivial atomic insulator to the system. For example, we take Eq. (2) and $L_x \cdot L_y$ being odd. Let us first consider a ground state $|GS_{\text{triv}}\rangle = \otimes_x |\hat{n}_x = 1\rangle$ of an atomic trivial insulator, which has $\langle \hat{U}_2 \rangle = 1$. When such a ground state is superposed with the topological state $|GS_{\text{top}}\rangle$, i.e., $|GS_{\text{new}}\rangle = |GS_{\text{top}}\rangle \otimes |GS_{\text{triv}}\rangle$, the quadrupole moment remains the same as before

$$\text{Im} \log \langle GS_{\text{top}} | \hat{U}_2 | GS_{\text{top}} \rangle = \text{Im} \log \langle GS_{\text{new}} | \hat{U}_2 | GS_{\text{new}} \rangle,$$

and hence showing the stability against addition of trivial bands (without turning on the coupling to the topological states).²⁵ This shows that our invariants Eq. (2) and Eq. (3) measure certain topological properties of the insulators. To further identify them as the “measure” for the multipoles, we need a few more steps.

1. Analytic Arguments: Now we argue that Eq. (2) and Eq. (3) are the physical multipole moments. We will concentrate on the quadrupole moment Eq. (2) for clarity. Below we choose our system to be on a torus $(x, y) \in [1, L_x] \times [1, L_y]$ and subject to the periodic boundary conditions $x + L_x \sim x$ and $y + L_y \sim y$.

First, we note that the Q_{xy} defined as above transforms correctly under the crystalline symmetries as the physical quadrupole moment. For example, under the mirrors $\{\mathcal{M}_x, \mathcal{M}_y\}$, we see that $\hat{U}_2 \rightarrow \hat{U}_2^*$, where asterisk denotes the complex conjugation, and thus $Q_{xy} \rightarrow -Q_{xy}$. When combined with the quantization “mod 1”, this enforces the allowed value of Q_{xy} to be 0 or $\frac{1}{2} \text{ mod } 1$, consistent with the nested Wilson loop approach.¹² (We defer a more careful analysis of the symmetry actions including C_4 symmetry to the supplemental material.²⁶)

Second, we can also intuitively understand why the polarization must vanish for the quadrupole moment to be well-defined. To this end, we perform $x \rightarrow x + L_x$

globally, which maps $\hat{U}_2 \rightarrow \hat{U}'_2 = \hat{U}_2 \hat{U}_{1;y}$ where $\hat{U}_{1;y} = \exp[2\pi i / L_y \sum_y y \hat{n}(\mathbf{r})] = \exp(2\pi i \hat{P}_y)$. Although $\langle \hat{U}_2 \rangle \neq \langle \hat{U}'_2 \rangle$ in general (because the ground state is not generally an eigenstate of $\hat{U}_{1;y}$), we find

$$\langle \hat{U}'_2 \rangle = \langle \hat{U}_2 \rangle \langle \hat{U}_{1;y} \rangle + \mathcal{O}\left(\frac{1}{E_{\text{gap}}}\right),$$

where E_{gap} is the excitation gap, which is inversely proportional to the correlation length.^{6,26,27} In the ideal limit $E_{\text{gap}} \rightarrow \infty$, we can see that the quadrupole moment, which is the imaginary part of $\langle \hat{U}_2 \rangle$, is well-defined when the polarization vanishes. Similarly, the total polarization \hat{P}_x along x must vanish to have a well-defined quadrupole moment. By passing, we note that this invariance of $\langle \hat{U}_2 \rangle$ up to the perturbative correction is weaker than the original Resta's formula Eq. (1) where $x \rightarrow x + L_x$ is an exact symmetry.²⁶ Though we have shown that the polarization at $E_{\text{gap}} \rightarrow \infty$ must vanish to have a well-defined quadrupole moment, the polarization is invariant under the adiabatic change of the gap when the quantizing symmetries present and thus the same conclusion should apply to the finite-gap systems.

Combining the above two arguments with the C_4 symmetry, we can demonstrate²⁶ that if $\langle \hat{U}_1 \rangle = 1$, $\langle \hat{U}_2 \rangle$ quantizes to ± 1 and if $\langle \hat{U}_1 \rangle = -1$, $\langle (\hat{U}_2)^2 \rangle$ is well-defined and quantizes to ± 1 . This allows us to use \hat{U}_2 for a (partial) many-body classification of generic C_4 -symmetric insulators²⁸⁻³⁰ beyond the topological quadrupolar insulator.

Finally, we can gain an important intuition from the phenomenological effective theory of the multipole moments. Using the standard field theory technique, we note

$$\langle GS | \hat{U}_a | GS \rangle = \text{Tr} \left[\frac{e^{-\beta H}}{\mathcal{Z}_0} \hat{U}_a \right] \Big|_{\beta \rightarrow \infty} \propto e^{i S_{\text{eff}}[A_{0;a}(\mathbf{r})]}, \quad (4)$$

in which $a = 1, 2, 3$ depends on the particular multipole that we are interested in, $A_{0;a}(\mathbf{r})$ is the gauge potential configuration generated by the unitary \hat{U}_a ,²⁶ and \mathcal{Z}_0 is the corresponding partition function. For the dipole case, we have

$$A_{0;a=1}(x, \tau) = 2\pi \frac{x}{L_x} \delta(\tau), \quad S_{\text{eff}} = \int_0^{L_x} dx \int_0^\beta d\tau P_x \cdot E_x.$$

Here we used the semi-classical electromagnetism response of the polarization $S_{\text{eff}} = \int \vec{P} \cdot \vec{E}$. Remarkably, despite of its semi-classical origin, we note that it is equivalent to the fully-quantum theory^{31,32} of one-dimensional topological insulator. Explicitly evaluating the value of the effective action, we find $\langle \hat{U}_1 \rangle \propto e^{2\pi i P_x}$. This can be further identified with the edge charge, which we derive by solving the equation of motion $q_{\text{edge}} = \int dx \frac{\delta \mathcal{L}_{\text{eff}}}{\delta A_0} = P_x$.

We generalize this to the quadrupole case, whose effec-

tive response is²⁶

$$S_{eff} = \int_0^{L_x} dx \int_0^{L_y} dy \int_0^\beta d\tau \frac{Q_{xy}}{2} (\partial_y E_x + \partial_x E_y), \quad (5)$$

where Q_{xy} is the physical quadrupole moment density and $E_{x,y}$ are electric fields. This effective theory captures the defining characteristics of the quadrupole insulator, including the corner charge and the charge current pattern generated from an adiabatic Thouless pumping.²⁶ Implementing $A_{0,a=2} = \frac{2\pi}{L_x L_y} xy \delta(\tau)$, we find $\langle \hat{U}_2 \rangle \propto e^{2\pi i Q_{xy}}$. It is straightforward to show that this quadrupole moment Q_{xy} is precisely the corner charge q_c , i.e., $Q_{xy} = q_c$, by solving the equation of motion for the probe gauge field δA_0 as done in the polarization case. Similar reasoning can be applied to the octupole case, too. In summary, our many-body invariants agree with the corner charges q_c , i.e., $\langle \hat{U}_a \rangle = \exp(2\pi i q_c)$, $a = 1, 2, 3$, which are the physical manifestation of the multipole moments even in the absence of quantizing symmetries.

- **Generalizations:** With the effective theory in hand, we can now generalize our invariants to arbitrary boundary condition, since the above relation Eq. (4) holds independently of which boundary condition being used. Furthermore, we can generalize the unitary \hat{U}_a to other unitaries saturating the effective action. For example, we can use

$$\hat{V}_1(l) = \begin{cases} \exp\left[\frac{2\pi i}{l} \sum_x x \hat{n}(x)\right] & \text{for } x \in [1, l] \\ 1 & \text{for } x \in (l, L_x], \end{cases} \quad (6)$$

to measure the polarization.²³ Here the whole system may be subject to the open boundary condition or to the periodic boundary condition. Similarly, we can define the generalized measure for the quadrupole moment as following:

$$\hat{V}_2(l) = \begin{cases} \exp\left[\frac{2\pi i}{l^2} \sum_{\mathbf{r}} xy \hat{n}(\mathbf{r})\right] & \text{for } \mathbf{r} \in [1, l] \times [1, l] \\ 1 & \text{otherwise.} \end{cases} \quad (7)$$

Again, the whole system may be subject to the periodic or open boundary conditions. We will see numerically that these operators work as good as the original formula.

- **Corner Charge, Nested Wilson Loop Index, and Multipole Moment:** Here we discuss a few related but distinct quantities by restricting ourselves to the quadrupolar case. (1) corner charge q_c , which is the total electric charge near the corner when the system is subject to the open boundary conditions. (2) Wannier-sector polarizations¹² $\{p_x^\omega, p_y^\omega\}$ (when they can be defined) and associated quadrupole moment $Q_{xy}^\omega = 2p_x^\omega p_y^\omega$, which are defined by nested Wilson loops, and (3) physical quadrupole moment Q_{xy}^{ph} . In general, all these three can be different from each other.

However, if the bulk and boundary-alone polarizations are absent (so that the quadrupole moments are well-defined) and if the quadrupolar charge distribution

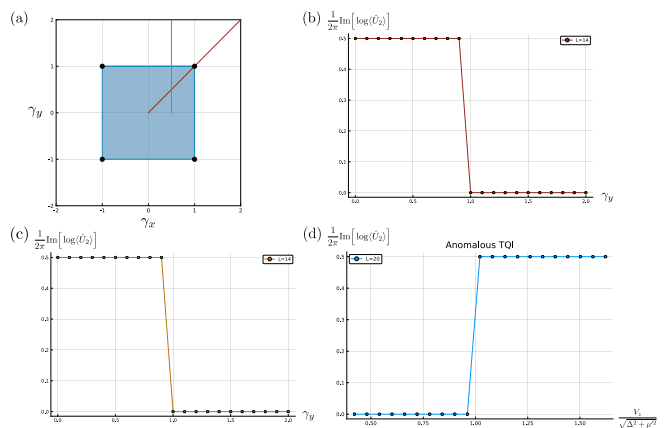


FIG. 1. (a) The phase diagram of the quadrupole insulator Eq. (8) when $\delta = 0$ and $\lambda_x = \lambda_y = 1$. The shaded region denotes topologically nontrivial phase (quadrupole moment equals 0.5) and black dots denote bulk energy gap closing points. (b) and (c) are evaluation of Q_{xy} Eq. (2) for the quadrupole insulator Eq. (8). We set $\lambda_x = \lambda_y = 1$ and $\delta = 0$, and evaluate Q_{xy} (b) along the cut $\gamma_x = \gamma_y$ and (c) along the cut $\gamma_x = 0.5$. We see in both cases there is a sharp change at $\gamma_y = 1$, which is consistent with the phase diagram (a). (d) Anomalous topological quadrupole insulator.¹⁹ Here, the ground state is known to be topological if $\frac{V_z}{\sqrt{\Delta^2 + \mu'^2}} > 1$ and trivial if $\frac{V_z}{\sqrt{\Delta^2 + \mu'^2}} < 1$, and this is well captured by \hat{U}_2 . See the supplemental material for details on the model and the numerical values of the parameters.²⁶

per unit cell is the only source of the corner charge, then the corner charge q_c would agree with a sensible quadrupole moment Q_{xy}^{ph} .¹² On the other hand, the nested Wilson loop index Q_{xy}^ω does not agree with q_c generally.¹² Hence, when the bulk-boundary correspondence^{33,34} holds, i.e., the boundary polarization in the systems of the open boundary condition is fully determined by the bulk quadrupole moments,¹² we expect generically

$$q_c \equiv Q_{xy}^{\text{ph}} \neq Q_{xy}^\omega,$$

in the absence of quantizing symmetries. In this regard, our key claim is that our many-body invariant Q_{xy} in Eq. (2) measures the physical observable $Q_{xy}^{\text{ph}} = q_c$, i.e., $Q_{xy} = Q_{xy}^{\text{ph}} = q_c$, which does not agree with the nested Wilson loop Q_{xy}^ω in the absence of quantizing symmetries. However, we remark that $Q_{xy} \neq Q_{xy}^\omega$ does not mean the failure of the nested Wilson loop indices because the indices are strictly defined only if there are quantizing symmetries. The similar reasoning generalizes to the octupolar case.

2. Numerical Proof: We now proceed to the numerical proof for our many-body invariants by testing the formula on the *non-interacting* topological quadrupolar states. We emphasize again here that, though the models are non-interacting, the invariant that we are computing is intrinsically a many-body quantity which requires

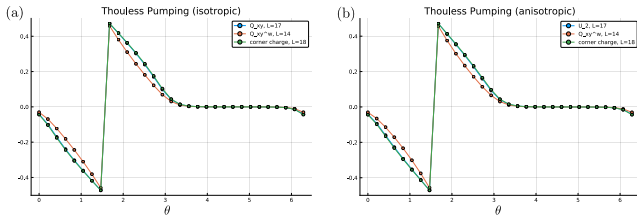


FIG. 2. Comparison between three different physical quantities, complex phase of $\langle \hat{U}_2 \rangle$, the quadrupole index Q_{xy}^ω , and corner charge q_c for (a) isotropic Thouless pumping Eq. (9) and (b) anisotropic Thouless pumping Eq. (10). While the complex phase of $\langle \hat{U}_2 \rangle$ and the corner charge q_c agree with each other with almost no discernible differences, the quadrupole index Q_{xy}^ω given in terms of the Wannier-sector polarizations agrees with the two only at $\theta = \pi/2, 3\pi/2$, i.e., $\delta = 0$ and the quadrupole moment is quantized.

the full knowledge of the many-body ground state. In the momentum basis, the Hamiltonian for the topological quadrupole insulator is

$$h(\mathbf{k}) = (\gamma_x + \lambda_x \cos(k_x))\Gamma_4 + \lambda_x \sin(k_x)\Gamma_3 + (\gamma_y + \lambda_y \cos(k_y))\Gamma_2 + \lambda_y \sin(k_y)\Gamma_1 + \delta \Gamma_0. \quad (8)$$

Here, $\Gamma_{a=0,\dots,4}$ is a proper set of gamma matrices.²⁶ When $\delta = 0$, there are two anti-commuting mirror symmetries \hat{M}_x and \hat{M}_y which quantize the quadrupole moment q_{xy} to either 0 or $1/2 \bmod 1$. If $\lambda_x = \lambda_y$ and $\gamma_x = \gamma_y$ are imposed (while keeping $\delta = 0$), there is a C_4 symmetry which also quantizes the quadrupole moment q_{xy} to either 0 or $1/2 \bmod 1$. $\delta \neq 0$ breaks both the mirror symmetries and C_4 symmetry, which quantize the quadrupoles, but C_2 symmetry remains intact which enforces the total polarization to vanish.

In FIG. 1, we present how the complex phase of $\langle \hat{U}_2 \rangle$ changes along different cuts in the parameter space of Eq. (8). The many-body invariant Eq. (2) reproduces the quantized quadrupole moments as well as the sharp phase transitions between topological and trivial quadrupole insulator, even when the bulk energy gap does not close at the transition point.

Given the success of our invariant in reproducing the phase diagram of Eq. (8), we applied it to the anomalous topological quadrupole insulator,¹⁹ where the naive application of the nested Wilson loop approach fails to predict the non-zero quantized quadrupole moments and the related phase transition. Here we find remarkably [see FIG. 1 (d)] that the expected quadrupole moment and phase transition are successfully reproduced with our many-body invariant \hat{U}_2 .

To define the quadrupole moment using the nested Wilson loop, the existence of the Wannier gap is crucial as we can then separate a Wannier band to evaluate the Wannier-sector polarization. In the case of Eq. (8) with $\delta = 0$, the phase transition between topological and trivial quadrupole insulator happens when the Wannier gap (instead of physical energy gap) closes and re-opens. On

the other hand, $|\langle \hat{U}_2 \rangle|$ always vanishes at phase boundary, where the Wannier gap closes i.e., $|\lambda_x/\gamma_x| = 1$ or $|\lambda_y/\gamma_y| = 1$ (Note that the physical gap closes only when $|\lambda_x/\gamma_x| = 1$ and $|\lambda_y/\gamma_y| = 1$). This highlights the relation between the Wannier gap and $|\langle \hat{U}_2 \rangle|$, and reminds the Resta's conjecture,^{6,35} which states that $|\langle \hat{U}_1 \rangle| \rightarrow 0$ as the energy gap $\rightarrow 0$ in the case of band or correlated insulators. We conjecture that $|\langle \hat{U}_2 \rangle|$ is related with the Wannier gap, i.e., $|\langle \hat{U}_2 \rangle| \rightarrow 0$ as the Wannier gap $\rightarrow 0$, and leave the detailed scaling study for the future research (see SM²⁶).

Having seen the success of \hat{U}_2 operator in detecting quantized quadrupole moment, we next ask what would happen if we break symmetries that protect the quantization of the quadrupole moment. In this case, the quantization of the quadrupole moment is lost and the quadrupole moment can take any value. However, due to the bulk-boundary correspondence,^{12,33,34} we expect that the corner charge is determined by the bulk quadrupole moment and so should be identical to the phase of $\langle \hat{U}_2 \rangle$. For numerical confirmations, we employ two Thouless pumping processes, one we call isotropic Thouless process and the other we call anisotropic Thouless process, where we relate three different quantities; a) the complex phase factor of $\langle \hat{U}_2 \rangle$ evaluated under full periodic boundary condition, b) the quadrupole index¹² $Q_{xy}^\omega = 2p_x^\omega p_y^\omega$ obtained from the nested Wilson loop, and c) the corner charge q_c localized at one corner under full open boundary condition. We note that the previous study¹² found numerically that b) and c) are not equivalent in the absence of the quantizing symmetries.

For the isotropic Thouless pumping case, we change the parameters in Eq. (8) according to

$$\begin{cases} \gamma_x = \gamma_y = 1 - 0.6 \sin(\theta) \\ \lambda_x = \lambda_y = 1 + 0.6 \sin(\theta) \\ \delta = 0.6 \cos(\theta) \end{cases}, \quad (9)$$

and for the anisotropic Thouless pumping process, we change the parameters according to

$$\begin{cases} \gamma_x = 1 - 0.6 \sin(\theta), & \gamma_y = 1 - 0.5 \sin(\theta) \\ \lambda_x = 1 + 0.6 \sin(\theta), & \lambda_y = 1 + 0.5 \sin(\theta) \\ \delta = 0.6 \cos(\theta) \end{cases}, \quad (10)$$

where $\theta \in [0, 2\pi]$ is the pumping parameter. In FIG. 2, we have plotted the three fundamentally different physical quantities for (a) isotropic and (b) anisotropic Thouless pumping processes. Apparent from the plots, we see almost no discernible difference between the complex phase factor of $\langle \hat{U}_2 \rangle$ and the corner charge q_c , indicating that the many-body invariant faithfully represents the physical quadrupole moment. On the other hand, the Wilson loop index Q_{xy}^ω differs from the two in general and agrees with the two only at quantized values. This is the numerical proof that \hat{U}_2 can measure the physical quadrupole moment density in a crystal.

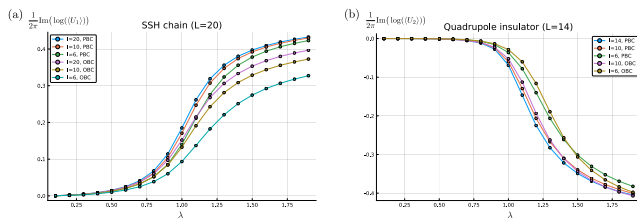


FIG. 3. Evaluation of the phase of $\langle \hat{V}_{\alpha=1,2}(l) \rangle$ of Eq. (6) and Eq. (7) for various values of l in the case of (a) Su-Schrieffer-Heeger chain and (b) Quadrupole insulator Eq. (8). We set $\gamma = 1.0$ ($\gamma_x = \gamma_y = 1.0$) and $\delta = 0.2$ and change λ ($= \lambda_x = \lambda_y$).

Next, we perform the numerical check for the generalized many-body invariants Eq. (6) and Eq. (7) in FIG. 3. We compute the phases of these invariants for various l 's for the Su-Schrieffer-Heeger chain³⁶ and topological quadrupolar insulators Eq. (8), which are both subject to the nonzero δ that breaks the quantization of polarization and quadrupole moments. For the Su-Schrieffer-Heeger chain, we have used

$$h_{\text{SSH}}(k) = \begin{pmatrix} \delta & \gamma + \lambda e^{-ik} \\ \gamma + \lambda e^{ik} & -\delta \end{pmatrix}.$$

Surprisingly, the overall trend is insensitive to which boundary condition is used and insensitive even when l is less than a half of the system size. Generically, we find that as l approaches the full system size and as the system size becomes large enough, these invariants collapse to the corner charge as we predicted. This completes the numerical proof of our generic many-body invariants.

Finally, we also have applied our invariant Eq. (2) to another model, the ‘‘boundary polarization model’’¹² supporting quantized corner charges $q_c = \pm 1/2$ yet having vanishing quadrupole moment (with suitable perturbations). Our invariant correctly captures the vanishing quadrupole moment despite of the nonzero corner charges coming from boundary-alone polarizations.²⁶ We also find several interesting numerical observations on \hat{U}_a including the dependence on coordinate parametrizations and scaling of $|\langle \hat{U}_2 \rangle|$, which we discuss in detail in supplemental materials.²⁶

3. Conclusions: We have proposed many-body invariants which work for both the quantized and non-quantized multipoles in crystalline many-body quantum states. Using analytical arguments, we showed that the invariants satisfy the expected behaviors, including symmetry-enforced quantization and stability against the addition of trivial states. Also we have demonstrated that these values can be identified with the corner charges of the higher-order topological insulators by utilizing the

effective theories of multipoles. Based on the reasonings of the effective field theories, we have provided an extension of our formulas, which work even for the case of open boundary condition. Finally, we provided numerical proof of our invariant by presenting explicit computations in toy models and confirmed that the invariants can measure the multipole moments.

Compared to the nested Wilson loop indices,¹² our invariants can measure the multipole moments even in the absence of quantizing symmetries and can be applied to interacting systems as well. On the other hand, in the presence of the quantizing symmetries, we have consistent results with the nested Wilson loop indices and provide complementary real-space formulation.

Let us mention a few possible extensions of our work. An obvious extension is to derive the nested Wilson-loop band indices for higher-order topological insulators from our many-body invariants Eq. (2) and Eq. (3), when there are proper quantizing symmetries. In the original work by Resta,⁵ the many-body invariant for polarization can be explicitly rewritten as the topological band index. We remark that, in general the nested Wilson-loop band indices disagree with the multipole moments defined by \hat{U}_a as we have discussed extensively, and thus the connection with the nested Wilson loop indices may not be straightforward. Also, it would be interesting to apply our work to the recent progresses in bosonic higher-order topological insulators.^{37,38} We believe that our invariants will naturally detect the underlying multipole moments whenever there exists a global $U(1)$ symmetry. Finally, it will be extremely desirable to connect our invariants to many-body pumping processes, which may potentially lead us to a novel Lieb-Schultz-Mattis theorem.²³

- *Note added:* Near finishing up this work, we are gratefully informed about an independent parallel work by William A. Wheeler, Lucas K. Wagner, and Taylor L. Hughes.³⁹ We appreciate their comments and for coordinating submission to arXiv. When their work and our work overlap, they agree with each other.

ACKNOWLEDGMENTS

We thank Akira Furusaki, Jung Hoon Han, Hyun Woong Kwon, Joel E. Moore, Masaki Oshikawa, Kwon Park, Shinsei Ryu, and Mike Zaletel for helpful discussions and comments. KS is supported by PRESTO, JST (JPMJPR18L4) and GYC is supported by BK 21 plus program at POSTECH in Korea. GYC thanks KIAS in Korea and RIKEN in Japan for their hospitality where some part of this work has been done. We thank Taylor Hughes for informing us about their parallel work³⁹ and sharing it with us before uploading to arXiv. We also thank Andrei Bernevig and Ben Wieder for their comments and explanation on nested Wilson loop indices.

- * Electronic Address: gilyoungcho@postech.ac.kr
- ¹ Raffaele Resta, “Macroscopic polarization in crystalline dielectrics: the geometric phase approach,” *Rev. Mod. Phys.* **66**, 899–915 (1994).
 - ² M. Z. Hasan and C. L. Kane, “Colloquium: Topological insulators,” *Rev. Mod. Phys.* **82**, 3045–3067 (2010).
 - ³ Xiao-Liang Qi and Shou-Cheng Zhang, “Topological insulators and superconductors,” *Rev. Mod. Phys.* **83**, 1057–1110 (2011).
 - ⁴ J. Zak, “Berry’s phase for energy bands in solids,” *Phys. Rev. Lett.* **62**, 2747–2750 (1989).
 - ⁵ Raffaele Resta, “Quantum-mechanical position operator in extended systems,” *Phys. Rev. Lett.* **80**, 1800–1803 (1998).
 - ⁶ Raffaele Resta and Sandro Sorella, “Electron localization in the insulating state,” *Phys. Rev. Lett.* **82**, 370–373 (1999).
 - ⁷ R. Nourafkan and G. Kotliar, “Electric polarization in correlated insulators,” *Phys. Rev. B* **88**, 155121 (2013).
 - ⁸ Masaaki Nakamura and Syngye Todo, “Order parameter to characterize valence-bond-solid states in quantum spin chains,” *Phys. Rev. Lett.* **89**, 077204 (2002).
 - ⁹ Gil Young Cho, Chang-Tse Hsieh, Takahiro Morimoto, and Shinsei Ryu, “Topological phases protected by reflection symmetry and cross-cap states,” *Phys. Rev. B* **91**, 195142 (2015).
 - ¹⁰ Hassan Shapourian, Ken Shiozaki, and Shinsei Ryu, “Many-body topological invariants for fermionic symmetry-protected topological phases,” *Phys. Rev. Lett.* **118**, 216402 (2017).
 - ¹¹ Wladimir A. Benalcazar, B. Andrei Bernevig, and Taylor L. Hughes, “Quantized electric multipole insulators,” *Science* **357**, 61–66 (2017).
 - ¹² Wladimir A. Benalcazar, B. Andrei Bernevig, and Taylor L. Hughes, “Electric multipole moments, topological multipole moment pumping, and chiral hinge states in crystalline insulators,” *Phys. Rev. B* **96**, 245115 (2017).
 - ¹³ Josias Langbehn, Yang Peng, Luka Trifunovic, Felix von Oppen, and Piet W. Brouwer, “Reflection-symmetric second-order topological insulators and superconductors,” *Phys. Rev. Lett.* **119**, 246401 (2017).
 - ¹⁴ Zhida Song, Zhong Fang, and Chen Fang, “ $(d - 2)$ -dimensional edge states of rotation symmetry protected topological states,” *Phys. Rev. Lett.* **119**, 246402 (2017).
 - ¹⁵ Frank Schindler, Ashley M. Cook, Maia G. Vergniory, Zhijun Wang, Stuart S. P. Parkin, B. Andrei Bernevig, and Titus Neupert, “Higher-order topological insulators,” *Science Advances* **4** (2018), 10.1126/sciadv.aat0346.
 - ¹⁶ Frank Schindler, Zhijun Wang, Maia G. Vergniory, Ashley M. Cook, Anil Murani, Shamashis Sengupta, Alik Yu Kasumov, Richard Deblock, Sangjun Jeon, Ilya Drozdov, Hlne Bouchiat, Sophie Guron, Ali Yazdani, B. Andrei Bernevig, and Titus Neupert, “Higher-order topology in bismuth,” *Nature Physics* **14**, 918 (2018).
 - ¹⁷ Motohiko Ezawa, “Minimal models for wannier-type higher-order topological insulators and phosphorene,” *Phys. Rev. B* **98**, 045125 (2018).
 - ¹⁸ Luka Trifunovic and Piet Brouwer, “Higher-order bulk-boundary correspondence for topological crystalline phases,” arXiv preprint arXiv:1805.02598 (2018).
 - ¹⁹ S. Franca, J. van den Brink, and I. C. Fulga, “An anomalous higher-order topological insulator,” *Phys. Rev. B* **98**, 201114 (2018).
 - ²⁰ Masaki Oshikawa and T. Senthil, “Fractionalization, topological order, and quasiparticle statistics,” *Phys. Rev. Lett.* **96**, 060601 (2006).
 - ²¹ Yuan-Ming Lu, Ying Ran, and Masaki Oshikawa, “Filling-enforced constraint on the quantized hall conductivity on a periodic lattice,” arXiv preprint arXiv:1705.09298 (2017).
 - ²² Masaki Oshikawa, “Commensurability, excitation gap, and topology in quantum many-particle systems on a periodic lattice,” *Phys. Rev. Lett.* **84**, 1535–1538 (2000).
 - ²³ Ian Affleck and Elliott H. Lieb, “A proof of part of haldane’s conjecture on spin chains,” *Letters in Mathematical Physics* **12**, 57–69 (1986).
 - ²⁴ Siddharth A. Parameswaran, Ari M. Turner, Daniel P. Arovas, and Ashvin Vishwanath, “Topological order and absence of band insulators at integer filling in non-symmorphic crystals,” *Nature Physics* **9**, 299 (2013).
 - ²⁵ For the systems with even $L_x \cdot L_y$, there is an additional minus sign (which can also be noticed in Resta’s original paper⁵) but the similar discussion can be straightforwardly made by noting that the topological part of the quadrupole moments are defined as the relative deviation from that of the trivial insulators.
 - ²⁶ See supplemental material for further details.
 - ²⁷ Haruki Watanabe and Masaki Oshikawa, “Inequivalent berry phases for the bulk polarization,” *Phys. Rev. X* **8**, 021065 (2018).
 - ²⁸ Hao Song, Sheng-Jie Huang, Liang Fu, and Michael Hermele, “Topological phases protected by point group symmetry,” *Phys. Rev. X* **7**, 011020 (2017).
 - ²⁹ Ken Shiozaki, Charles Zhaoxi Xiong, and Kiyonori Gomi, “Generalized homology and atiyah-hirzebruch spectral sequence in crystalline symmetry protected topological phenomena,” arXiv preprint arXiv:1810.00801 (2018).
 - ³⁰ Zhida Song, Chen Fang, and Yang Qi, “Real-space recipes for general topological crystalline states,” arXiv preprint arXiv:1810.11013 (2018).
 - ³¹ Jeffrey Goldstone and Frank Wilczek, “Fractional quantum numbers on solitons,” *Phys. Rev. Lett.* **47**, 986–989 (1981).
 - ³² Xiao-Liang Qi, Taylor L. Hughes, and Shou-Cheng Zhang, “Topological field theory of time-reversal invariant insulators,” *Phys. Rev. B* **78**, 195424 (2008).
 - ³³ David Vanderbilt and R. D. King-Smith, “Electric polarization as a bulk quantity and its relation to surface charge,” *Phys. Rev. B* **48**, 4442–4455 (1993).
 - ³⁴ Jun-Won Rhim, Jan Behrends, and Jens H. Bardarson, “Bulk-boundary correspondence from the intercellular zak phase,” *Phys. Rev. B* **95**, 035421 (2017).
 - ³⁵ Ryohei Kobayashi, Yuya O. Nakagawa, Yoshiki Fukusumi, and Masaki Oshikawa, “Scaling of the polarization amplitude in quantum many-body systems in one dimension,” *Phys. Rev. B* **97**, 165133 (2018).
 - ³⁶ W. P. Su, J. R. Schrieffer, and A. J. Heeger, “Solitons in polyacetylene,” *Phys. Rev. Lett.* **42**, 1698–1701 (1979).
 - ³⁷ Yizhi You, Trithep Devakul, F. J. Burnell, and Titus Neupert, “Higher-order symmetry-protected topological states for interacting bosons and fermions,” *Phys. Rev. B* **98**, 235102 (2018).
 - ³⁸ Oleg Dubinkin and Taylor L. Hughes, “Higher order bosonic topological phases in spin models,” arXiv preprint arXiv:1807.09781 (2018).

- ³⁹ William A. Wheeler, Lucas K. Wagner, and Taylor L. Hughes, “Many-body electric multipole operators in extended systems,” arXiv preprint arXiv:1812.06990 (2018).

Supplemental Materials for “Many-Body Invariants for Multipoles in Higher-Order Topological Insulators”

Byungmin Kang

School of Physics, Korea Institute for Advanced Study, Seoul 02455, Korea

Ken Shiozaki

Yukawa Institute for Theoretical Physics, Kyoto University, Kyoto 606-8502, Japan

Gil Young Cho

Department of Physics, Pohang University of Science and Technology (POSTECH), Pohang 37673, Republic of Korea

(Dated: December 15, 2024)

CONTENTS

A. Details on Symmetry Properties of \hat{U}_2	2
1. Large Translation Symmetry	2
2. C_4 Symmetry and Mirrors	2
B. \hat{U}_a as Many-Body Indices for Crystalline Insulators	2
1. Dipole Operator \hat{U}_1	3
a. $1d$ bosonic SPT phases with $U(1) \times \mathbb{Z}_2^R$ symmetry	3
b. $1d$ fermionic SPT phases with $U(1) \times \mathbb{Z}_2^R$ symmetry	3
2. Quadrupole Operator \hat{U}_2	4
a. With C_4 symmetry	4
b. $2d$ bosonic SPT phases with $U(1) \times \mathbb{Z}_4^{C_4}$ symmetry	5
c. $2d$ fermionic SPT phases with $U(1) \times \mathbb{Z}_4^{C_4}$ symmetry	6
C. Details on Effective Field Theory of Quadrupole Moments	7
1. Derivation of Effective Action: Multipolar Electromagnetism	7
2. Corner Charge and Thouless Pumping	8
a. Corner Charge	8
b. Thouless Pumping	9
3. From $\langle GS \hat{U}_a GS \rangle$ to Partition Functions	9
D. Details on Tight-Binding Models	10
1. Su-Schrieffer-Heeger chain	10
2. Topological Quadrupole insulator	11
a. Symmetries of the tight-binding model	11
b. Mirror symmetries	11
c. C_4 symmetry	12
d. C_2 symmetry	12
e. Symmetry breaking perturbations	12
3. Topological Octupolar Insulator	12
a. Evaluation of $\langle \hat{U}_3 \rangle$	13
4. Anomalous Topological Quadrupolar Insulator	13
5. Edge-localized polarization model	13
E. Miscellaneous Observations on Many-Body Invariants	14
1. Scaling of $ \langle \hat{U}_a \rangle $	15
a. Scaling of $ \langle \hat{U}_1 \rangle $	15
b. Scaling of $ \langle \hat{U}_2 \rangle $	15
2. Dependence on Coordinate Parameterization	16
References	17

Appendix A: Details on Symmetry Properties of \hat{U}_2

In this section, we present the details of the symmetry actions on the many-body invariants in \hat{U}_2 . This highlights under what conditions \hat{U}_2 is well-defined and yields a quantized value when evaluated with respect to a quantum many-body state. To be specific, we discuss the action of the crystalline C_4 symmetry on the many-body invariant and the large translation symmetry.

1. Large Translation Symmetry

Here we provide the details of the large coordinate translation operation $x \rightarrow x + L_x$ (with L_x being the system size along x -direction) on the many-body quadrupole invariant Eq. (2) in the main text. As noted in the main text, we find

$$x \rightarrow x + L_x : \quad \hat{U}_2 \rightarrow \hat{U}_2 \hat{U}_{1;y} \quad (\text{A1})$$

where $\hat{U}_{1;y}$ is the many-body measure for the polarization along y direction. Now the key step that we used in the main text is

$$\begin{aligned} \langle \hat{U}_2 \rangle &= \langle \hat{U}_2 \rangle \langle \hat{U}_{1;y} \rangle + \mathcal{O}\left(\frac{\epsilon_0}{E_{\text{gap}}}\right), \\ &= \langle \hat{U}_2 \rangle \langle \hat{U}_{1;y} \rangle + \mathcal{O}\left(\frac{\xi}{a_0}\right), \end{aligned} \quad (\text{A2})$$

where ϵ_0 and a_0 are the unit energy and unit scale which make the expressions dimensionless. From the first line to the second line, we used the fact that $\frac{1}{E_{\text{gap}}} \propto \xi$ with ξ being the correlation length. When the correlation length becomes an atomic scale $\xi \rightarrow 0^+$ (ultra-short correlated), i.e., the ideal atomic insulator limit, we see that $\langle \hat{U}_2 \rangle = \langle \hat{U}_2 \rangle \langle \hat{U}_1 \rangle$ which enforces $\langle \hat{U}_1 \rangle = 1$.

The above equations can be derived from the following observation:

$$\hat{U}_1 |GS\rangle = \langle \hat{U}_1 \rangle |GS\rangle + \mathcal{O}\left(\frac{\epsilon_0}{E_{\text{gap}}}\right), \quad (\text{A3})$$

which is a slight rewriting of Eq. (37) in Ref. [1].

2. C_4 Symmetry and Mirrors

With the discussion above, we now discuss the action of C_4 on \hat{U}_2 for the domain $\mathcal{M} = [1, L_x] \times [1, L_y]$. Obviously the system respects the C_4 symmetry only when $L_x = L_y = L$. Furthermore, it is not difficult to see that the domain $\mathcal{M} = [1, L] \times [1, L]$ is transformed into $\mathcal{M}' = [-L, -1] \times [1, L]$. Hence, we find that

$$C_4 : \hat{U}_2 \rightarrow \hat{U}_2^* \hat{U}_{1;x}. \quad (\text{A4})$$

Since, in the ideal limit $\xi \rightarrow 0$, $\langle \hat{U}_2^* \hat{U}_{1;x} \rangle = \langle \hat{U}_2^* \rangle \langle \hat{U}_{1;x} \rangle = \langle \hat{U}_2^* \rangle$ (with vanishing polarization) and thus $\langle \hat{U}_2 \rangle = \langle \hat{U}_2^* \rangle$. This enforces $Q_{xy} = -Q_{xy}$ consistent with the previous work². In fact, even for the mirror symmetries $M_x \times M_y$ discussed in the main text, extra factors of $\hat{U}_{1;\mu=x,y}$'s do show up because of the transformations on the domain \mathcal{M} , which need to be included. Nevertheless, the conclusion made in the main text remains the same, i.e., C_4 or mirrors flip the sign of Q_{xy} , which can be explicitly seen in our many-body invariants in an appropriate limit.

Appendix B: \hat{U}_a as Many-Body Indices for Crystalline Insulators

Here we provide the details of taking \hat{U}_a 's as the many-body invariants for generic crystalline insulators. We start with a brief warm-up with the polarization operator on the one-dimensional cases with the reflections and then move to the quadrupole operator in two dimensions with C_4 symmetry. Within this section, we assume the ultra-short correlated ground states, i.e., the correlation length $\xi \rightarrow 0^+$.

1. Dipole Operator \hat{U}_1

Let S^1 be a 1d ring with a length L_x . We introduce a lift $S^1 \rightarrow \mathbb{R}, x \mapsto \tilde{x}$. With this, we define the dipole operator

$$\hat{P}_1 := \frac{1}{L_x} \int_0^{L_x} d\tilde{x} \tilde{x} \hat{\rho}(\tilde{x}). \quad (\text{B1})$$

Here, $\hat{\rho}(\tilde{x})$ is the $U(1)$ charge density operator extended on \mathbb{R}

$$\hat{\rho}(\tilde{x}) = \sum_{n \in \mathbb{Z}} \sum_j \delta(x - x_j + nL_x) \hat{n}_j, \quad (\text{B2})$$

where \hat{n}_j takes values in integers \mathbb{Z} . A change of lift is a change of the interval $[0, L_x] \mapsto [n_x L_x, (n_x + 1)L_x]$ with $n_x \in \mathbb{Z}$, which induces

$$\hat{P}_1 \mapsto \frac{1}{L_x} \int_{n_x L_x}^{(n_x+1)L_x} d\tilde{x} \tilde{x} \hat{\rho}(\tilde{x}) = \hat{P}_1 + n_x \hat{N}, \quad (\text{B3})$$

where $\hat{N} := \sum_j \hat{n}_j$ is the total charge in S^1 . Since \hat{N} takes values in integers, we find that \hat{P}_1 module 1 is well-defined operator. Put differently,

$$\hat{U}_1 := \exp\left(\frac{2\pi i}{L_x} \int_0^{L_x} d\tilde{x} \tilde{x} \hat{\rho}(\tilde{x})\right) \quad (\text{B4})$$

is well-defined.

The reflection \hat{R} send a dof at $x_j \in S^1$ to one at $-x_j \in S^1$, i.e. $\hat{R} \hat{\rho}(\tilde{x}) \hat{R}^{-1} = \hat{\rho}(-\tilde{x})$. We have

$$\hat{R} \hat{P}_1 \hat{R}^{-1} = -\hat{P}_1 \pmod{1}. \quad (\text{B5})$$

a. 1d bosonic SPT phases with $U(1) \times \mathbb{Z}_2^R$ symmetry

The dipole operator can be used to diagnose SPT phases. Let us consider bosonic SPT phases with $U(1)$ and reflection symmetry, where reflection commutes with $U(1)$. The classification is given by $\mathbb{Z} \times \mathbb{Z}_2 \times \mathbb{Z}_2$. Let b_x be complex boson annihilation operator with a unit charge. At the reflection center, we denote the reflection even/odd bosons by $b_{x,\pm}$. Each abelian group is generated as

$$\mathbb{Z} : b_{0,+}^\dagger, \quad \mathbb{Z}_2 : b_{0,+}^\dagger b_{0,-}, \quad \mathbb{Z}_2 : b_{0,+}^\dagger b_{L_x/2,+}. \quad (\text{B6})$$

(It is easy to derive it by the use of the real-space Atiyah-Hirzebruch spectral sequence (AHSS).³⁻⁵) In addition to the dipole operator, the $U(1)$ charge \hat{N} and reflection \hat{R} are also many-body topological invariants. Here is the table of the relationship between topological invariants and generating models.

	\hat{N}	$\frac{1}{\pi i} \ln \hat{R} \pmod{2}$	$2\hat{P}_1 \pmod{2}$
$b_{0,+}^\dagger$	1	0	0
$b_{0,+}^\dagger b_{0,-}$	0	1	0
$b_{0,+}^\dagger b_{L_x/2,+}$	0	0	1

The set of topological invariants $(\hat{N}, \hat{R}, \hat{P}_1)$ completely classifies SPT phases.

b. 1d fermionic SPT phases with $U(1) \times \mathbb{Z}_2^R$ symmetry

Let us consider fermionic 1d SPT phases on S^1 with $U(1)$ and reflection symmetry. We assume the reflection does not change the $U(1)$ charge. The classification is known to be $\mathbb{Z} \times \mathbb{Z}_2 \times \mathbb{Z}_4$. Let f_x be complex fermion annihilation operator with a unit charge. At the reflection center, we denote the reflection even/odd fermions by $f_{x,\pm}$. Each direct summand is generated as

$$\mathbb{Z} : f_{0,+}^\dagger, \quad \mathbb{Z}_2 : f_{0,+}^\dagger f_{0,-}, \quad \mathbb{Z}_4 : f_{0,+}^\dagger f_{L_x/2,+}. \quad (\text{B7})$$

In addition to the dipole operator, the fermion number \hat{N} and reflection \hat{R} are also many-body topological invariants. Here is the table of topological invariants and generating models.

	\hat{N}	$\frac{1}{\pi i} \ln \hat{R} \pmod{2}$	$2\hat{P}_1 \pmod{2}$
$f_{0,+}^\dagger$	1	0	0
$f_{0,+}^\dagger f_{0,-}$	0	1	0
$f_{0,+}^\dagger f_{L_x/2,+}$	0	0	1

Note that the dipole operator \hat{U}_1 is insufficient to diagnose the \mathbb{Z}_4 SPT phase. We need a \mathbb{Z}_4 many-body topological invariant. A candidate of \mathbb{Z}_4 invariant is the partial reflection.⁶

2. Quadrupole Operator \hat{U}_2

Let T^2 be a 2d real-space torus with lengths L_x and L_y for x and y directions. We introduce a lift $T^2 \rightarrow \mathbb{R}^2, (x, y) \mapsto (\tilde{x}, \tilde{y})$. Let $\hat{\rho}(\tilde{x}, \tilde{y})$

$$\hat{\rho}(\tilde{x}, \tilde{y}) = \sum_{n_x, n_y \in \mathbb{Z}} \sum_j \delta(x - x_j + n_x L_x) \delta(y - y_j + n_y L_y) \hat{n}_j \quad (\text{B8})$$

be charge density operator extended to \mathbb{R}^2 . We define the dipole operators

$$\hat{P}_{1,x} := \frac{1}{L_x} \int_0^{L_x} d\tilde{x} \int_0^{L_y} d\tilde{y} \tilde{x} \hat{\rho}(\tilde{x}, \tilde{y}) \pmod{1}, \quad (\text{B9})$$

$$\hat{P}_{1,y} := \frac{1}{L_y} \int_0^{L_x} d\tilde{x} \int_0^{L_y} d\tilde{y} \tilde{y} \hat{\rho}(\tilde{x}, \tilde{y}) \pmod{1}. \quad (\text{B10})$$

These are well-defined modulo 1. We shall define the quadrupole operator

$$\hat{P}_2 := \frac{1}{L_x L_y} \int_0^{L_x} d\tilde{x} \int_0^{L_y} d\tilde{y} \tilde{x} \tilde{y} \hat{\rho}(\tilde{x}, \tilde{y}). \quad (\text{B11})$$

Let us consider the condition for \hat{P}_2 being well-defined. Under a change of lift labeled by $(n_x, n_y) \in \mathbb{Z}^2$, \hat{P}_2 changes as

$$\hat{P}_2 \mapsto \frac{1}{L_x L_y} \int_{n_x L_x}^{(n_x+1)L_x} d\tilde{x} \int_{n_y L_y}^{(n_y+1)L_y} d\tilde{y} \tilde{x} \tilde{y} \hat{\rho}(\tilde{x}, \tilde{y}) \quad (\text{B12})$$

$$= \hat{P}_2 + n_x \hat{P}_{1,y} + n_y \hat{P}_{1,x} + n_x n_y \hat{N} \quad (\text{B13})$$

$$= \hat{P}_2 + n_x \hat{P}_{1,y} + n_y \hat{P}_{1,x} \pmod{1}. \quad (\text{B14})$$

Therefore, the range of \hat{P}_2 depends on the dipole operators.

a. With C_4 symmetry

With C_4 -rotation symmetry, the quadrupole operator enjoys an interesting relationship. Let $L = L_x = L_y$ be the length of a side of the torus. The C_4 -rotation acts on the density operator as $\hat{C}_4 \hat{\rho}(\tilde{x}, \tilde{y}) \hat{C}_4^{-1} = \hat{\rho}(-\tilde{y}, \tilde{x})$. First, we notice that the dipole operator for x direction is related with that for y direction by the C_4 rotation

$$\hat{C}_4 \hat{P}_{1,x} \hat{C}_4^{-1} = -\hat{P}_{1,y}. \quad (\text{B15})$$

Using this relation twice, we find $\hat{C}_2 \hat{P}_{1,x} \hat{C}_2^{-1} = -\hat{P}_{1,x}$, meaning that $\hat{P}_{1,x}$ is quantized into $\{0, \frac{1}{2}\}$. We write $\hat{P}_1 = \hat{P}_{1,x} = \hat{P}_{1,y} \pmod{1}$. On the quadrupole operator, the C_4 rotation induces

$$\hat{C}_4 \hat{P}_2 \hat{C}_4^{-1} = \frac{1}{L^2} \int_0^L d\tilde{x} \int_0^L d\tilde{y} \tilde{x} \tilde{y} \hat{\rho}(-\tilde{y}, \tilde{x}) \quad (\text{B16})$$

$$= \frac{1}{L^2} \int_0^{-L} d\tilde{x} \int_0^L d\tilde{y} \tilde{x} \tilde{y} \hat{\rho}(\tilde{x}, \tilde{y}) \quad (\text{B17})$$

$$= -\hat{P}_2 - \hat{P}_1. \quad (\text{B18})$$

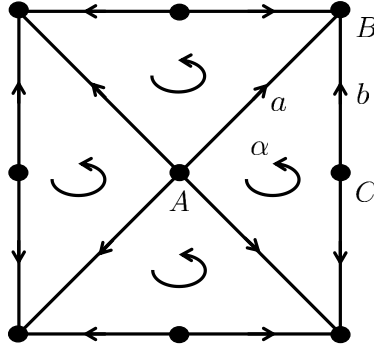


FIG. 1. A cell decomposition of the 2-torus with the C_4 -rotation symmetry.

Combining (B14) with this, we conclude that (i) when $\hat{P}_1 = 0$, \hat{P}_2 is well-defined module 1 and takes values in $\{0, \frac{1}{2}\}$, or (ii) when $\hat{P}_1 = \frac{1}{2}$, \hat{P}_2 is well-defined module $\frac{1}{2}$ and takes values in $\{0, \frac{1}{4}\}$. It should be noted that the quadrupole operator \hat{P}_2 behaves as a \mathbb{Z}_4 invariant. A model with $(\hat{P}_1, \hat{P}_2) = (\frac{1}{2}, \frac{1}{4})$ is the generator of \mathbb{Z}_4 .

Let us apply the quadrupole operator to diagnosing SPT phases with C_4 -rotation symmetry.

b. 2d bosonic SPT phases with $U(1) \times \mathbb{Z}_4^{C_4}$ symmetry

The quadrupole operator may serves as a many-body topological invariant diagnosing the SPT phases. Let us consider 2d bosonic SPT phases with $U(1)$ and C_4 -rotation symmetry preserving the $U(1)$ charge. The classification of SPT phases is readily obtained by the real-space AHSS. We introduce the C_4 symmetric cell decomposition of the 2d torus as shown in Fig. 1 [a]. The E^1 -page of the AHSS^{4,5} is given as in the following table.

$$\begin{array}{c|ccc}
 n=0 & (\mathbb{Z} \times \mathbb{Z}_4) \times (\mathbb{Z} \times \mathbb{Z}_4) \times (\mathbb{Z} \times \mathbb{Z}_2) & \mathbb{Z} \times \mathbb{Z} & \\
 n=1 & 0 & 0 & 0 \\
 n=2 & & \mathbb{Z}^{\times 2} \times \mathbb{Z}^{\times 2} & \mathbb{Z}^{\times 2} \\
 \hline
 E_{p,-n}^1 & \{A, B, C\} & \{a, b\} & \{\alpha\} \\
 & p=0 & p=1 & p=2
 \end{array} \tag{B19}$$

Here, we showed the only contents in the E^1 -page relevant to the SPT phases. At the 0-cell A , $\mathbb{Z} \times \mathbb{Z}_4 \subset E_{0,0}^1$ is characterized by the $U(1)$ charge and the C_4 eigenvalue, respectively. At the 2-cell α , $E_{2,-2}^1 = \mathbb{Z}^{\times 2}$ are generated by bosonic quantum Hall state and E_8 state, respectively. The first differential $d_{p,-n}^1 : E_{p,-n}^1 \rightarrow E_{p-1,-n}^1$ is defined as trivializing SPT phases at $(p-1)$ -cells by adiabatically crated SPT phases on p -cells. Because of the bosonic commutation relation, the C_4 -symmetric quartet $q = b_1 b_2 b_3 b_4$ with $\hat{C}_4 b_j \hat{C}_4^{-1} = b_{j+1}$ has the trivial C_4 -charge $\hat{C}_4 q \hat{C}_4^{-1} = q$. This is also true for the C_2 -symmetric doublet. We have

$$d_{1,0}^1 = \frac{\begin{array}{c|cc} a & b & \\ \mathbb{Z} & \mathbb{Z} & \\ \hline -4 & 0 & \mathbb{Z} \quad A \\ 0 & 0 & \mathbb{Z}_4 \\ \hline 4 & 4 & \mathbb{Z} \quad B \\ 0 & 0 & \mathbb{Z}_4 \\ \hline 0 & -2 & \mathbb{Z} \quad C \\ 0 & 0 & \mathbb{Z}_2 \end{array}}{\quad}, \quad d_{2,-2}^1 = 0. \tag{B20}$$

Taking the homology of d^1 , we have the E^2 -page

$$\begin{array}{c|ccc}
 n = 0 & \mathbb{Z} \times \mathbb{Z}_2^{\times 2} \times \mathbb{Z}_4^{\times 3} & 0 & \\
 n = 1 & 0 & 0 & 0 \\
 n = 2 & & & \mathbb{Z}^{\times 2} \\
 \hline
 E_{p,-n}^2 & p = 0 & p = 1 & p = 2
 \end{array} \tag{B21}$$

This is the limiting page. The group extension as an abelian group is trivial. The classification of SPT phases is found to be $\mathbb{Z}^{\times 3} \times \mathbb{Z}_2^{\times 2} \times \mathbb{Z}_4^{\times 3}$.

Let us focus on the subgroup $E_{0,0}^2 = \mathbb{Z} \times \mathbb{Z}_2^{\times 2} \times \mathbb{Z}_4^{\times 3}$ composed of atomic insulators. Let $b(x, y)$ be complex boson annihilation operator with a unit charge. At the C_n -rotation center, we denote bosons with rotation eigenvalue λ by $b_{C_n=\lambda}(x, y)$. From the E^1 -page and the first differential $d_{1,0}^1$, generating models of $E_{0,0}^2$ are found as

$$\mathbb{Z} : g_1 = b_{C_4=1}^\dagger(0, 0), \tag{B22}$$

$$\mathbb{Z}_4 : g_2 = b_{C_4=i}^\dagger(0, 0)b_{C_4=1}(0, 0), \tag{B23}$$

$$\mathbb{Z}_4 : g_3 = b_{C_4=i}^\dagger\left(\frac{L}{2}, \frac{L}{2}\right)b_{C_4=1}\left(\frac{L}{2}, \frac{L}{2}\right), \tag{B24}$$

$$\mathbb{Z}_4 : g_4 = b_{C_4=1}(0, 0)b_{C_4=1}^\dagger\left(\frac{L}{2}, \frac{L}{2}\right), \tag{B25}$$

$$\mathbb{Z}_2 : g_5 = b_{C_2=-1}^\dagger\left(\frac{L}{2}, 0\right)b_{C_2=1}\left(\frac{L}{2}, 0\right)b_{C_2=-1}^\dagger\left(0, \frac{L}{2}\right)b_{C_2=1}\left(0, \frac{L}{2}\right), \tag{B26}$$

$$\mathbb{Z}_2 : g_6 = b_{C_4=1}(0, 0)b'_{C_4=1}(0, 0)b_{C_2=1}^\dagger\left(\frac{L}{2}, 0\right)b_{C_2=1}^\dagger\left(0, \frac{L}{2}\right). \tag{B27}$$

In the last line, $b_{C_4=1}(0, 0)$ and $b'_{C_4=1}(0, 0)$ represent different flavors of bosons. Here is the table of the relationship between topological invariants and generating models.

Classification	Generator	\hat{N}	$\frac{2}{\pi i} \ln \hat{C}_4 \pmod{4}$	$2\hat{P}_1 \pmod{2}$	$4\hat{P}_2 \pmod{4}$
\mathbb{Z}	g_1	1	0	0	0
\mathbb{Z}_4	g_2	0	1	0	0
\mathbb{Z}_4	g_3	0	1	0	0
\mathbb{Z}_4	g_4	0	0	1	{1, 3}
\mathbb{Z}_2	g_5	0	2	0	0
\mathbb{Z}_2	g_6	0	0	1	0

The set of topological invariants $(\hat{N}, \hat{C}_4, \hat{P}_1, \hat{P}_2)$ is insufficient to completely classify SPT phases. In particular, it is impossible to distinguish the generating models g_2, g_3 , and g_5 from each others.

c. 2d fermionic SPT phases with $U(1) \times \mathbb{Z}_4^{C_4}$ symmetry

Next, we consider 2d fermionic SPT phases with $U(1)$ and C_4 -rotation symmetry where C_4 preserves the $U(1)$ charge. The AHSS is parallel to that for bosonic ones. We have the same E^1 -page as (B19). Due to the fermionic anticommutation relation, the first differential $d_{1,0}^1$ changes to

$$d_{1,0}^1 = \frac{\begin{array}{c|cc} a & b & \\ \mathbb{Z} & \mathbb{Z} & \\ \hline -4 & 0 & \mathbb{Z} \ A \\ 2 & 0 & \mathbb{Z}_4 \\ \hline 4 & 4 & \mathbb{Z} \ B \\ 2 & 2 & \mathbb{Z}_4 \\ \hline 0 & -2 & \mathbb{Z} \ C \\ 0 & 1 & \mathbb{Z}_2 \end{array}}{\quad}, \quad d_{2,-2}^1 = 0. \tag{B28}$$

Taking the homology of d^1 , we have the E^2 -page

$$\begin{array}{c|cc}
n=0 & \mathbb{Z} \times \mathbb{Z}_2^{\times 2} \times \mathbb{Z}_4^{\times 2} \times \mathbb{Z}_8 & 0 \\
n=1 & & 0 \quad 0 \\
n=2 & & \mathbb{Z}^{\times 2} \\
\hline
E_{p,-n}^2 & p=0 & p=1 \quad p=2
\end{array} \tag{B29}$$

This is the limiting page. The group extension as an abelian group is trivial. The classification of SPT phases is found to be $\mathbb{Z}^{\times 3} \times \mathbb{Z}_2^{\times 2} \times \mathbb{Z}_4^{\times 2} \times \mathbb{Z}_8$.

Let us focus on the subgroup $E_{0,0}^2 = \mathbb{Z} \times \mathbb{Z}_2^{\times 2} \times \mathbb{Z}_4^{\times 2} \times \mathbb{Z}_8$ composed of atomic insulators. Let $f(x, y)$ be complex boson annihilation operator with a unit charge. At the C_n -rotation center, we denote fermions with rotation eigenvalue λ by $f_{C_n=\lambda}(x, y)$. The generating models of $E_{0,0}^2$ are given as

$$\mathbb{Z} : g_1 = (1, 0, 0, 0, 0, 0)^T = f_{C_4=1}^\dagger(0, 0), \tag{B30}$$

$$\mathbb{Z}_4 : g_2 = (0, 1, 0, 0, 0, 0)^T = f_{C_4=i}^\dagger(0, 0)f_{C_4=1}(0, 0), \tag{B31}$$

$$\mathbb{Z}_2 : g_3 = (0, 0, 0, 0, 0, 1)^T = f_{C_2=-1}^\dagger\left(\frac{L}{0}, 0\right)f_{C_2=1}\left(\frac{L}{2}, 0\right)f_{C_2=-1}^\dagger\left(0, \frac{L}{0}\right)f_{C_2=1}\left(0, \frac{L}{2}\right), \tag{B32}$$

$$\mathbb{Z}_8 : g_4 = (-1, 0, 1, 0, 0, 0)^T = f_{C_4=1}^\dagger\left(\frac{L}{2}, \frac{L}{2}\right)f_{C_4=1}(0, 0), \tag{B33}$$

$$\mathbb{Z}_2 : g_5 = (-2, -1, 2, 1, 0, 0)^T = f_{C_4=i}^\dagger\left(\frac{L}{2}, \frac{L}{2}\right)f_{C_4=1}^\dagger\left(\frac{L}{2}, \frac{L}{2}\right)f_{C_4=i}(0, 0)f_{C_4=1}(0, 0), \tag{B34}$$

$$\mathbb{Z}_4 : g_6 = (-2, 0, 0, 0, 1, 0)^T = f_{C_2=-1}^\dagger\left(\frac{L}{2}, 0\right)f_{C_2=-1}^\dagger\left(0, \frac{L}{2}\right)f_{C_4=1}(0, 0)f'_{C_4=1}(0, 0), \tag{B35}$$

$$\tag{B36}$$

Here, $f_{C_4=1}(0, 0)$ and $f'_{C_4=1}(0, 0)$ represent different flavors of fermions. Here is the table of the relationship between topological invariants and generating models.

Classification	Generator	\hat{N}	$\frac{2}{\pi i} \ln \hat{C}_4 \pmod{4}$	$2\hat{P}_1 \pmod{2}$	$4\hat{P}_2 \pmod{4}$
\mathbb{Z}	g_1	1	0	0	0
\mathbb{Z}_4	g_2	0	1	0	0
\mathbb{Z}_2	g_3	0	2	0	0
\mathbb{Z}_8	g_4	0	0	1	{1, 3}
\mathbb{Z}_2	g_5	0	0	0	2
\mathbb{Z}_4	g_6	0	0	1	0

The set of topological invariants $(\hat{N}, \hat{C}_4, \hat{P}_1, \hat{P}_2)$ is insufficient to completely classify SPT phases. The quadrupole operator \hat{P}_2 can distinguish, for example, the g_4 phase from the g_6 phase.

Appendix C: Details on Effective Field Theory of Quadrupole Moments

In this section, we provide the details of the effective field theory for the quadrupole insulators. We first derive the effective response from the semi-classical picture and then use it to reproduce the quintessential features⁷ of the topological quadrupole insulators. Furthermore, we also show the link between the ground state expectation value $\langle \hat{U}_a \rangle$ and the partition function. Although we mainly focus on the quadrupolar case, let us remark that all the discussions here can be straightforwardly generalized to the octupolar and higher-polar cases.

1. Derivation of Effective Action: Multipolar Electromagnetism

We start from the effective responses for electric multipoles. First, the uniform monopole or charge density ρ in a spatial region \mathcal{M} has the following response:

$$S_{eff} = \int_{\mathcal{M}} d\tau d^d r \rho V(\mathbf{r}) \tag{C1}$$

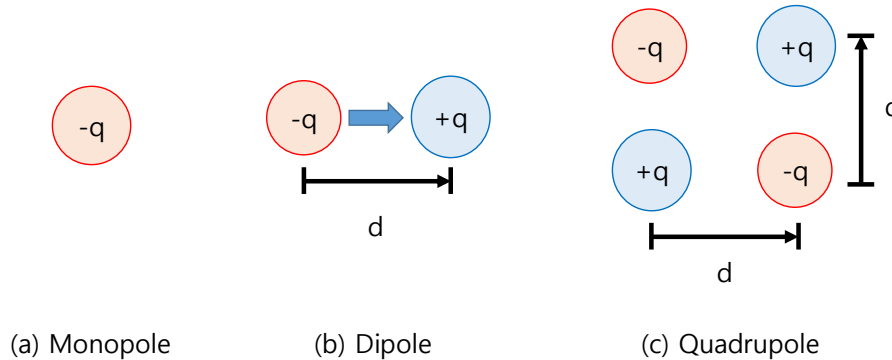


FIG. 2. Charge configuration in real space with non-vanishing (a) charge, (b) dipole, and (c) quadrupole moment.

Second, a single dipole at the site \mathbf{r} with the magnitude $\vec{P} = q\mathbf{d}$ has the following response:

$$S_{\text{dipole}} = \int d\tau q [V(\mathbf{r} + \mathbf{d}) - V(\mathbf{r})] \approx \int d\tau q\mathbf{d} \cdot \partial V(\mathbf{r}) = \int d\tau \vec{P} \cdot \vec{E}. \quad (\text{C2})$$

Hence, when there are uniform polarization density \vec{p} over the area \mathcal{M} , we find

$$S_{\text{eff}} = \int_{\mathcal{M}} d\tau d^d r \vec{p} \cdot \vec{E}. \quad (\text{C3})$$

Third, a single quadrupole $Q_{xy} = qd^2$ at the site $\mathbf{r} = (x, y)$ (see Fig. 2) has the following response:

$$\begin{aligned} S_{\text{quadrupole}} &= \int d\tau q [V(x, y) - V(x + d, y) - V(x, y + d) + V(x + d, y + d)] \approx \int d\tau qd^2 \partial_x \partial_y V(x, y) \\ &= \int d\tau \frac{Q_{xy}}{2} [\partial_x E_y + \partial_y E_x]. \end{aligned} \quad (\text{C4})$$

Thus, when there are uniform quadrupole density Q_{xy} over the area \mathcal{M} , we find

$$S_{\text{eff}} = \int_{\mathcal{M}} d\tau d^d r \frac{Q_{xy}}{2} [\partial_x E_y + \partial_y E_x], \quad (\text{C5})$$

which is the effective action used in the main text.

It is not difficult to show that the uniform octupole density O_{xyz} over the region \mathcal{M} has the following response:

$$S_{\text{eff}} = \int_{\mathcal{M}} d\tau d^d r \frac{O_{xyz}}{3} [\partial_x \partial_y E_z + \partial_z \partial_y E_x + \partial_z \partial_x E_y]. \quad (\text{C6})$$

2. Corner Charge and Thouless Pumping

From the effective action for the quadrupole Eq. (C5), we can reproduce the essential features⁷ of the topological quadrupole insulators. For this, let us consider a rectangular region $\mathcal{M} = [-L_x, L_x] \times [-L_y, L_y]$ with uniform quadrupole density $Q_{xy} \neq 0$, and the vacuum ($Q_{xy} = 0$) outside \mathcal{M} as described in Fig. 3 (a).

a. Corner Charge

We first compute the corner charge, which can be done by computing the equation of motion for A_0 in the effective response.

$$\rho(\mathbf{r}) = \frac{\delta \mathcal{L}_{\text{eff}}}{\delta A_0(\mathbf{r})} = \partial_x \partial_y Q_{xy} \quad (\text{C7})$$

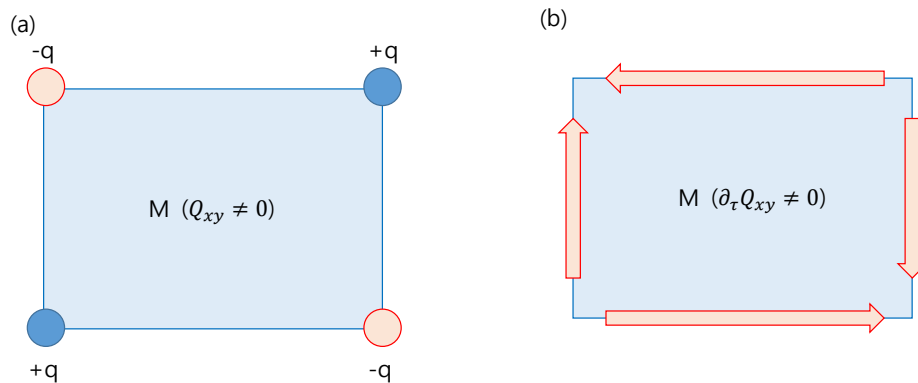


FIG. 3. (a) Corner charges of quadrupole insulator derived from the effective action. Charges are only localized at four corners of the rectangular region \mathcal{M} , where \mathcal{M} has nonzero quadrupole moment density Q_{xy} and is surrounded by the vacuum with trivial quadrupole moment. (b) Charge current configuration derived from the effective action under the Thouless pumping. In this case, charges flow only along the boundary of \mathcal{M} and their directions are denoted as arrows.

Obviously, the RHS of the above equation, $\partial_x \partial_y Q_{xy}$, is non-zero only at the corners of \mathcal{M} . Hence, we find

$$\rho(\mathbf{r}) = Q_{xy} \left[\delta(x - L_x) \delta(y - L_y) - \delta(x + L_x) \delta(y - L_y) - \delta(x - L_x) \delta(y + L_y) + \delta(x + L_x) \delta(y + L_y) \right]. \quad (\text{C8})$$

This is consistent with the intuitive picture of the corner charge generated from the quadrupole moment density. Integrating over a quadrant of the \mathcal{M} , we finally find that

$$q_c = \pm Q_{xy}, \quad (\text{C9})$$

whose sign depends on which quadrant of the space being integrated over.

b. Thouless Pumping

Next, we imagine that the uniform quadrupole moment density Q_{xy} depends on time, i.e., we have $Q_{xy} = Q_{xy}(\tau)$. This allows the charge currents to flow along the boundary of the topological quadrupole insulators. To see this, we calculate

$$J_x = \frac{\delta \mathcal{L}_{eff}}{\delta A_x} = -\partial_y \partial_\tau Q_{xy}, \quad J_y = \frac{\delta \mathcal{L}_{eff}}{\delta A_y} = -\partial_x \partial_\tau Q_{xy}, \quad (\text{C10})$$

which is essentially equivalent to the charge flow in the process of Thouless pumping in the topological quadrupole insulator, obtained in Ref. [7]. Note that the current flows along the boundary of \mathcal{M} during the Thouless pumping, which is shown in FIG. 3 (b).

3. From $\langle GS | \hat{U}_a | GS \rangle$ to Partition Functions

Here we relate the ground state overlaps and the partition functions, which has been extensively used in many-body invariants for symmetry-protected topological states^{8,9} on the relation of the ground state expectation values of the symmetry operators and the partition functions. This is in fact a small variation of the standard Dyson formula, which can be found in any quantum field theory text books.

We first start with noting that

$$|GS\rangle = \frac{1}{\sqrt{Z}} \sum_n e^{-\frac{\beta}{2} H} |n\rangle, \quad Z = \text{Tr}[e^{-\beta H}], \quad (\text{C11})$$

where the true ground state can be obtained by letting the ‘‘temperature’’ $1/\beta \rightarrow 0$. This implies that

$$\langle GS | \hat{U}_a | GS \rangle \propto \frac{1}{Z} \sum_n \langle n | e^{-\frac{\beta}{2} H} \hat{U}_a e^{-\frac{\beta}{2} H} | n \rangle = \frac{1}{Z} \text{Tr} \left[e^{-\beta H} \hat{U}_a \right]. \quad (\text{C12})$$

Now, in order to relate Eq. (C12) to the effective functional against the gauge potential configuration set by \hat{U}_a , we need to properly interpret the partition function in the RHS of Eq. (C12). Pictorially, this can be represented as the imaginary time evolution (See Fig. 4). For a proper interpretation, let us break the partition function into the two parts. The first part is the action of \hat{U}_a . Note that these \hat{U}_a 's involve complex phase factors proportional to the particle number, i.e., $\hat{U}_a \sim \exp[i\phi(\mathbf{r})\hat{n}(\mathbf{r})]$ (with $\phi(\mathbf{r})$ depending on a). This means that \hat{U}_a appearing on the partition function Eq. (C12) is the same as the action of the gauge potential $A_0(\mathbf{r}, \tau)$ on the states at $\tau = 0$, i.e., $A_0(\mathbf{r}, \tau) \propto \delta(\tau)$. In the second part, we act $\exp(-\beta H)$, which is the imaginary time-evolution on the states after the action of \hat{U}_a .

Because the RHS of Eq. (C12) can be interpreted as the evolution of the states under the gauge potentials, the RHS should be equivalent to the following:

$$\langle GS|\hat{U}_a|GS\rangle \sim |Z| \exp\left(iS_{eff}[A_0(\mathbf{r}, \tau)]\right), \quad (\text{C13})$$

in which $S_{eff}[A_0(\mathbf{r}, \tau)]$ is the effective response against $A_0(\mathbf{r}, \tau)$, which is set by \hat{U}_a . Here, we also used the fact that the multipolar electromagnetic responses are *topological* (or Berry phase) because they involve a single time-derivative $\sim \partial_\tau$. Thus, this multipolar response against $A_0(\mathbf{r}, \tau)$ contributes to the imaginary part of the $\langle \hat{U}_a \rangle$. With all these ingredients, it is straightforward to confirm that our many-body invariants are designed to saturate $S_{eff} = 2\pi Q_{xy}$ for the quadrupole case and $2\pi P_x$ for the dipole case.

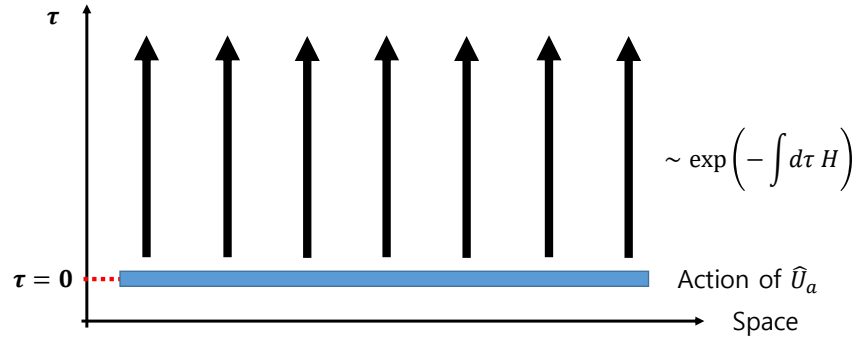


FIG. 4. Interpretation of the partition functions with the insertion of \hat{U}_a . \hat{U}_a acts at $\tau = 0$ followed by the imaginary time evolution along τ . Periodic boundary condition with period β is used along τ direction.

Appendix D: Details on Tight-Binding Models

In this section, we summarize the physical properties and the symmetries of the tight-binding models for the topological insulators appearing in the main text.

1. Su-Schrieffer-Heeger chain

A minimal model for one-dimensional crystalline topological insulator is the Su-Schrieffer-Heeger (SSH) chain¹⁰ which is a tight-binding model having alternating “weak” and “strong” hopping terms:

$$H_{SSH} = \sum_r \left[(\gamma c_{r,1}^\dagger c_{r,2} + \lambda c_{r,2}^\dagger c_{r+1,1} + \text{h.c.}) + \delta (c_{r,1}^\dagger c_{r,1} - c_{r,2}^\dagger c_{r,2}) \right], \quad (\text{D1})$$

where $c_{r,\alpha=1,2}^\dagger$ is the electron creation operator at site r orbital α , γ and λ are intra- and inter-site hopping strengths, and δ is the onsite potential strength. Under the periodic boundary condition, it is convenient to work with the Bloch

basis:

$$c_{\mathbf{k},\alpha}^\dagger = \frac{1}{\sqrt{L}} \sum_{r=1}^L e^{-ikr} c_{r,\alpha}^\dagger, \quad (\text{D2})$$

where $k = \frac{2\pi n}{L}$ for some $n \in \mathbb{Z}$, $\alpha = 1, 2$ is the orbital index, and L is the system size. $c_{k,\alpha}$ can be defined analogously. The block Hamiltonian in terms of the Bloch state is given by

$$h_{\text{SSH}}(k) = \begin{pmatrix} \delta & \gamma + \lambda e^{ik} \\ \gamma + \lambda e^{-ik} & -\delta \end{pmatrix}. \quad (\text{D3})$$

2. Topological Quadrupole insulator

A minimal model for topological quadrupole insulator⁷, is given by

$$H = \sum_{\mathbf{r}} \left[\gamma_x (c_{\mathbf{r},1}^\dagger c_{\mathbf{r},3} + c_{\mathbf{r},2}^\dagger c_{\mathbf{r},4} + \text{h.c.}) + \gamma_y (c_{\mathbf{r},1}^\dagger c_{\mathbf{r},4} - c_{\mathbf{r},2}^\dagger c_{\mathbf{r},3} + \text{h.c.}) + \lambda_x (c_{\mathbf{r},1}^\dagger c_{\mathbf{r}+\hat{x},3} + c_{\mathbf{r},4}^\dagger c_{\mathbf{r}+\hat{x},2} + \text{h.c.}) \right. \\ \left. + \lambda_y (c_{\mathbf{r},1}^\dagger c_{\mathbf{r}+\hat{y},4} - c_{\mathbf{r},3}^\dagger c_{\mathbf{r}+\hat{y},2} + \text{h.c.}) + \delta (c_{\mathbf{r},1}^\dagger c_{\mathbf{r},1} + c_{\mathbf{r},2}^\dagger c_{\mathbf{r},2} - c_{\mathbf{r},3}^\dagger c_{\mathbf{r},3} - c_{\mathbf{r},4}^\dagger c_{\mathbf{r},4}) \right], \quad (\text{D4})$$

where $c_{\mathbf{r},\alpha}^\dagger$ and $c_{\mathbf{r},\alpha}$ are the fermion creation and annihilation operator at site $\mathbf{r} = (x, y)$ and $\alpha = 1, 2, 3, 4$ is the orbital index. If we impose the periodic boundary condition along x - and y -direction then it is convenient to work with the Bloch (momentum) basis

$$c_{\mathbf{k},\alpha}^\dagger = \frac{1}{\sqrt{L_x L_y}} \sum_{x=1}^{L_x} \sum_{y=1}^{L_y} e^{-i\mathbf{k}\cdot\mathbf{r}} c_{\mathbf{r},\alpha}^\dagger,$$

where $\mathbf{k} = (k_x, k_y) = (\frac{2\pi n_x}{L_x}, \frac{2\pi n_y}{L_y})$ for some $n_x, n_y \in \mathbb{Z}$ is the Bloch momentum, $\alpha = 1, 2, 3, 4$ is the orbital index, and L_x and L_y are the system sizes along x - and y -direction. $c_{\mathbf{k},\alpha}$ is defined analogously. Using the Bloch basis, the Hamiltonian Eq. (D4) takes the block diagonal form

$$h(\mathbf{k}) = (\gamma_x + \lambda_x \cos(k_x))\Gamma_4 + \lambda_x \sin(k_x)\Gamma_3 + (\gamma_y + \lambda_y \cos(k_y))\Gamma_2 + \lambda_y \sin(k_y)\Gamma_1 + \delta \Gamma_0, \quad (\text{D5})$$

where $\Gamma_0 = \tau_3 \otimes \tau_0$, $\Gamma_i = -\tau_2 \otimes \tau_i$ for $i = 1, 2, 3$, $\Gamma_4 = \tau_1 \otimes \tau_0$, where τ_0 is the 2×2 identity matrix and τ_i is the i th Pauli matrix. When $\delta = 0$, the physical energy band spectrum is gapless only when $|\gamma_x/\lambda_x| = 1$ and $|\gamma_y/\lambda_y| = 1$ while the Wannier gap closes when $|\gamma_x/\lambda_x| = 1$ or $|\gamma_y/\lambda_y| = 1$. The ground state at half-filling becomes a topological quadrupole insulator when $\delta = 0$, $|\gamma_x/\lambda_x| < 1$ and $|\gamma_y/\lambda_y| < 1$.

a. Symmetries of the tight-binding model

When $\delta = 0$ in Eq. (D4), there exists various symmetries which quantize the quadrupole moment $q_{xy} = 0, 1/2 \pmod{1}$. In the following, we summarize the symmetries of Eq. (D4) in the case of $\delta = 0$.

b. Mirror symmetries

With respect to the Bloch basis, x - and y -mirror symmetry can be written as

$$\hat{M}_x = i\tau_1 \otimes \tau_3 \quad \text{and} \quad \hat{M}_y = i\tau_1 \otimes \tau_1, \quad (\text{D6})$$

and the block Hamiltonian Eq. (D5) transforms as

$$\hat{M}_x h(k_x, k_y) \hat{M}_x^{-1} = h(-k_x, k_y) \quad \text{and} \quad \hat{M}_y h(k_x, k_y) \hat{M}_y^{-1} = h(k_x, -k_y). \quad (\text{D7})$$

Because of the π flux threaded in each plaquette, two mirror symmetries do not commute but anticommute: $\{\hat{M}_x, \hat{M}_y\} = 0$.

c. C_4 symmetry

When $\lambda_x = \lambda_y$ and $\gamma_x = \gamma_y$ in addition to $\delta = 0$, there exists C_4 symmetry which also quantizes q_{xy} . With respect to the Bloch basis, the C_4 symmetry can be represented as

$$\hat{r}_4 = \begin{pmatrix} 0 & \tau_0 \\ -i\tau_2 & 0 \end{pmatrix} \quad (\text{D8})$$

and also

$$\hat{r}_4 h(k_x, k_y) \hat{r}_4^{-1} = h(k_y, -k_x) \quad (\text{D9})$$

holds.

d. C_2 symmetry

Even when $\delta \neq 0$, there exists C_2 symmetry which quantizes the polarization in x - and y -direction. So when $|\delta|$ is small compared to other parameters in Eq. (D5), both x and y polarization are 0 hence the quadrupole moment q_{xy} is well-defined although it is no-longer quantized. With respect to the Bloch basis, the C_2 operator can be represented as

$$\hat{r}_2 = -i\tau_0 \otimes \tau_2, \quad (\text{D10})$$

and also

$$\hat{r}_2 h(\mathbf{k}) \hat{r}_2^{-1} = h(-\mathbf{k}) \quad (\text{D11})$$

holds.

e. Symmetry breaking perturbations

Here, we present how onsite symmetry breaking perturbations affect the bulk quadrupole moment, defined as a complex phase of $\langle \hat{U}_2 \rangle$, when perturbing away from a topological quadrupole insulator point. In adding perturbations, we still want to keep C_2 symmetry as this would enforce the quantization of polarization in x - and y -direction, i.e., total polarization remains zero when the perturbation is small.

Starting from the C_2 operator Eq. (D10), one can classify 4×4 matrices that commute with \hat{r}_2 . The general form of such matrix can be expressed as

$$H_{\text{pert}} = \begin{pmatrix} a_r \tau_0 + c_r \tau_2 & e_c \tau_0 + f_c \tau_2 \\ e_c^* \tau_0 + f_c^* \tau_2 & b_r \tau_0 + d_r \tau_2 \end{pmatrix}, \quad (\text{D12})$$

where a_r, b_r, c_r, d_r are real parameters, e_c and f_c are complex parameters, and asterisk denotes the complex conjugation. One can immediately see that the δ term in Eq. (D5) is reproduced when $a_r = -b_r = \delta$ and set all the other coefficients to zero in Eq. (D12). Let us also note that when $(a_r = b_r = 0, c_r = -d_r, e_c = -if_c \in \mathbb{R})$, Eq. (D12) preserves two mirror symmetries and when $(a_r = b_r = 0, c_r = d_r, e_c = -if_c \in \mathbb{R})$, Eq. (D12) preserves C_4 symmetry.

One can check numerically that when the perturbation Eq. (D12) is *onsite*, only nonzero a_r and b_r do change the quadrupole moment whereas other terms do not. When a_r and b_r are nonzero, we can always add an identity matrix with suitable coefficient so that the perturbation reduces to the δ term in Eq. (D5). Hence Eq. (D5) is quite generic.

3. Topological Octupolar Insulator

A minimal model for an octupole insulator is given by⁷

$$\begin{aligned} h_{\text{octupole}}(\mathbf{k}) = & \lambda_y \sin(k_y) \Gamma'_1 + [\gamma_y + \lambda_y \cos(k_y)] \Gamma'_2 + \lambda_x \sin(k_x) \Gamma'_3 \\ & + [\gamma_x + \lambda_x \cos(k_x)] \Gamma'_4 + \lambda_z \sin(k_z) \Gamma'_5 + [\gamma_z + \lambda_z \cos(k_z)] \Gamma'_6, \end{aligned} \quad (\text{D13})$$

where $\Gamma'_i = \sigma_3 \otimes \Gamma_i$ for $i = 0, 1, 2, 3$ with Γ_i being the same set of Gamma matrices appearing in Eq. (D5), $\Gamma'_4 = \sigma_1 \otimes I_{4 \times 4}$, $\Gamma'_5 = \sigma_2 \otimes I_{4 \times 4}$, $\Gamma'_6 = i\Gamma'_0 \Gamma'_1 \Gamma'_2 \Gamma'_3 \Gamma'_4 \Gamma'_5$, and $\gamma_{x,y,z}$ and $\lambda_{x,y,z}$ are intra- and inter-site hopping strengths. When $|\lambda_i| > |\gamma_i|$ for all $i = x, y, z$, the half-filled ground state has topologically nontrivial octupole moment.

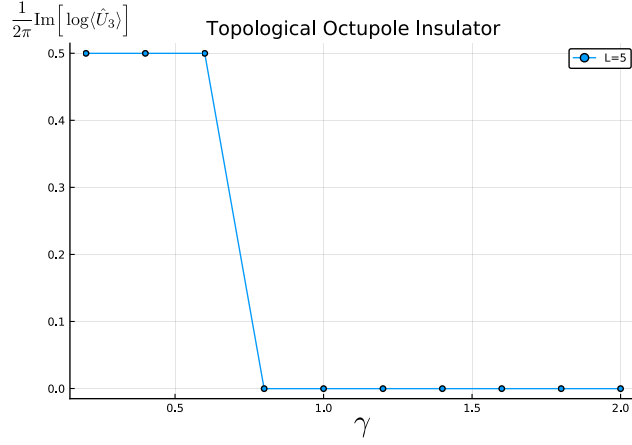


FIG. 5. The complex phase of $\langle\hat{U}_3\rangle$ for topological octupole insulator Eq. (D13). We set $\lambda_x = \lambda_y = \lambda_z = 1.0$ and tune $\gamma \equiv \gamma_x = \gamma_y = \gamma_z \in [0, 2]$. When $\gamma < 1.0$ ($\gamma > 1.0$), the ground state is in topological (trivial) octupole phase, which is indeed captured by $\langle\hat{U}_3\rangle$ up to finite-size effects.

a. Evaluation of $\langle\hat{U}_3\rangle$

Here we present the numerical evaluation of the expectation value of \hat{U}_3 with respect to the half-filled ground state of the octupole insulator Eq. (D13). As done in the quadrupole insulator case, which is summarized in the FIG. 1 in the main text, we change the parameter through the phase transition between the topological octupole insulator and the trivial insulator, as shown in Fig. 5.

4. Anomalous Topological Quadrupolar Insulator

A minimal model for an anomalous topological quadrupole insulator is given by Ref. [11].

$$H_{\text{ATQI}}(\mathbf{k}) = [2t_x(1 - \cos(k_x)) - \mu]\sigma_3 \otimes \sigma_0 \otimes \sigma_0 + V_z\sigma_0 \otimes \sigma_3 \otimes \sigma_0 + \Delta\sigma_1 \otimes \sigma_0 \otimes \sigma_0 \\ + \alpha \sin(k_x)\sigma_3 \otimes \sigma_2 \otimes \sigma_0 - [\beta_1 - \beta_2 \cos(k_y)]\sigma_3 \otimes \sigma_1 \otimes \sigma_2 - \beta_2 \sin(k_y)\sigma_3 \otimes \sigma_1 \otimes \sigma_1, \quad (\text{D14})$$

where t_x is the nearest neighbor hopping strength in x -direction, μ is the chemical potential, V_z is the Zeeman energy, Δ is the superconducting pairing strength, α and β_1/β_2 are the Rashba spin-orbit coupling strengths in x - and y -direction. In the main text, we set $(t_x, \mu, \Delta, \alpha, \beta_1, \beta_2) = (1.7, -0.9, 1.6, 3.7, 0.8, 6.2)$ and tune $V_z \in [0.7, 2.7]$. When $V_z > \sqrt{\Delta^2 + \mu'^2}$, the half-filled ground state is topologically nontrivial and when $V_z < \sqrt{\Delta^2 + \mu'^2}$, the half-filled ground state is trivial where $\mu' \approx 0.46$ for our choices of parameters.

5. Edge-localized polarization model

One of the key characteristic of the quadrupole insulator is that the following four physical observables are identical: $q_c = |p_x^{\text{edge}}| = |p_y^{\text{edge}}| = Q_{xy}$, where q_c is the corner charge localized at one edge in the case of full open boundary condition, $p_{x(y)}^{\text{edge}}$ is edge localized polarization along x -direction (y -direction) in the case of open boundary condition along x -direction (y -direction) and periodic boundary condition along y -direction (x -direction), and Q_{xy} is the bulk quadrupole moment. In contrast, there exists model, *edge-localized polarization* model, in which $q_c = |p_x^{\text{edge}}| + |p_y^{\text{edge}}|$ and $Q_{xy} = 0$ instead. A minimal model for this edge-localized polarization model is given by⁷

$$h(\mathbf{k}) = \begin{pmatrix} \delta\tau_0 & q(\mathbf{k}) \\ q^\dagger(\mathbf{k}) & -\delta\tau_0 \end{pmatrix}, \\ q(\mathbf{k}) = \begin{pmatrix} \gamma + \lambda_x e^{ik_x} & \gamma + \lambda_y e^{ik_y} \\ \gamma + \lambda_y e^{-ik_y} & \gamma + \lambda_x e^{-ik_x} \end{pmatrix}, \quad (\text{D15})$$

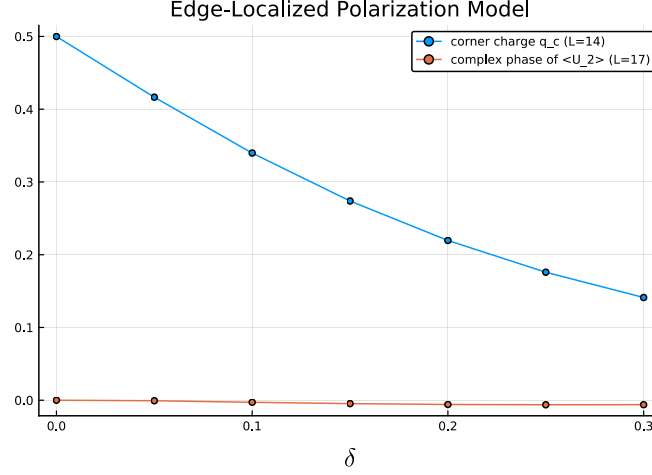


FIG. 6. Edge-localized polarization model Eq. (D15) with $(\gamma, \lambda_x, \lambda_y) = (0.1, 1.0, 0.5)$ and change $\delta \in [0, 0.3]$. The corner charge comes solely from the boundary localized polarization and the bulk quadrupole moment vanishes. We indeed see that the complex phase of $\langle \hat{U}_2 \rangle$ is trivial up to finite size effects.

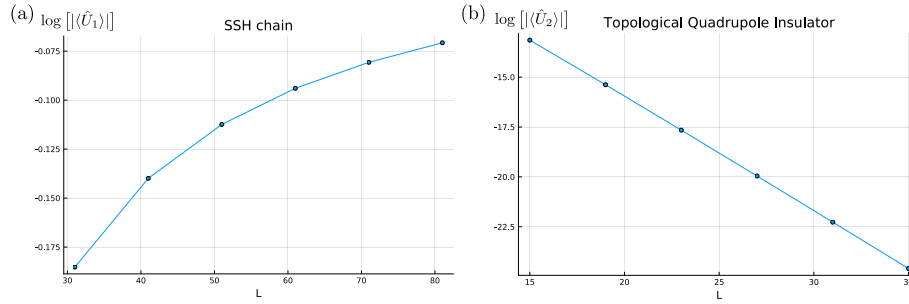


FIG. 7. Scaling of many-body invariants $|\langle \hat{U}_{n=1,2} \rangle|$ versus the linear system size L in the case of (a) SSH chain Eq. (D3) with $(\gamma, \lambda, \delta) = (1.0, 2.0, 0.1)$ and (b) topological quadrupole insulator Eq. (D5) with $(\gamma_x, \gamma_y, \lambda_x, \lambda_y, \delta) = (1.0, 1.0, 2.0, 2.0, 0.1)$. (a) The modulus of $\langle \hat{U}_1 \rangle$ converges to 1 as $L \rightarrow \infty$, as expected in the case of a gapped insulator. (b) The modulus of $\langle \hat{U}_2 \rangle$ decays exponentially in L even in the case of a gapped insulator.

where τ_0 is the 2×2 identity matrix and γ and λ are intra- and inter-layer hopping strengths. To see our many-body invariant \hat{U}_2 Eq. (E4) indeed not sensitive to the edge-localized polarization that is not coming from the bulk quadrupole moment, we numerically compute the complex phase of $\langle \hat{U}_2 \rangle$ for the minimal model Eq. (D15). In FIG. 6, we set $(\gamma, \lambda_x, \lambda_y) = (0.1, 1.0, 0.5)$ and change $\delta \in [0, 0.3]$. As we tune δ , the corner charge changes and equals $|p_x^{\text{edge}}| + |p_y^{\text{edge}}|$, while the bulk quadrupole moment vanishes. As we can be seen in the figure, the complex phase of $\langle \hat{U}_2 \rangle$ is trivial, hence capturing the vanishing bulk quadrupole moment.

Appendix E: Miscellaneous Observations on Many-Body Invariants

Here we present several miscellaneous observations on many-body invariants. This includes the scaling behavior of $|\langle \hat{U}_a \rangle|$ and the dependence on the coordinate parametrizations. To be concrete, we concentrate on operators for the polarization \hat{U}_1 and quadrupole moment \hat{U}_2 .

1. Scaling of $|\langle \hat{U}_a \rangle|$

a. Scaling of $|\langle \hat{U}_1 \rangle|$

Here we summarize the known scaling forms of the modulus of the expectation value of \hat{U}_1 , which is introduced by Resta [12]. For an one-dimensional system with system size L , the Resta's operator is given by

$$\hat{U}_1 = \exp\left(\frac{2\pi i}{L} \sum_{x=1}^L x \hat{n}_x\right), \quad (\text{E1})$$

where $\hat{n}_x = \sum_{\alpha} c_{x,\alpha}^{\dagger} c_{x,\alpha}$ is the occupation number operator at site x with α being the orbital index, and we label the position at site x to $x = 1, 2, \dots, L$. Eq. (E1) is well-defined in the sense that upon re-labeling a position x by $x + L$, \hat{U}_1 remains invariant. Moreover, in the case of a band insulator, the expectation value of \hat{U}_1 is related to the Zak phase by (up to an additional minus sign which we address in detail below)

$$\frac{1}{2\pi} \text{Im}[\log \langle \hat{U}_1 \rangle] = \int_{\text{BZ}} dk \text{tr}(\mathcal{A}_k) + \mathcal{O}(1/L) \text{ mod } 1, \quad (\text{E2})$$

where the expectation value in the LHS is with respect to the many-body ground state, the integral in the RHS is the Zak phase¹³ with BZ denoting the one dimensional Brillouin zone, \mathcal{A}_k is the Berry connection, and $\mathcal{O}(1/L)$ term vanishes as the system size $L \rightarrow \infty$. This provides a proof that the phase of the expectation value of \hat{U}_1 detects the polarization, as the polarization is equal to the Zak phase in a proper unit.

Although the complex phase of $\langle \hat{U}_1 \rangle$ gives the electric polarization, its modulus also captures invaluable information, e.g., the localization length of the ground state¹⁴. In FIG. 7, we provide the scaling of (a) $|\langle \hat{U}_1 \rangle|$ for the SSH chain Eq. (D3) with $(\gamma, \lambda, \delta) = (1.0, 2.0, 0.1)$ versus the linear system size L . In this case, the bulk gap is finite. As expected, when the linear system size $L \rightarrow \infty$, $|\langle \hat{U}_1 \rangle| \rightarrow 1$ in the case of the SSH chain. In general, when the bulk gap is nonzero, the modulus of the expectation value $|\langle \hat{U}_1 \rangle|$ converges to a positive number as $L \rightarrow \infty$. On the other hand, at critical point $|\langle \hat{U}_1 \rangle|$ vanishes as $L \rightarrow \infty$ and it is conjectured to obey the following scaling relation¹⁵:

$$|\langle \hat{U}_1 \rangle| \sim \frac{1}{L^{\beta}}, \quad (\text{E3})$$

where $\beta > 0$ is the exponent characterizing the decay in the thermodynamic limit.

b. Scaling of $|\langle \hat{U}_2 \rangle|$

Here we perform the scaling study of $|\langle \hat{U}_2 \rangle|$ with respect to the length and the Wannier gap. Recall that \hat{U}_2 is

$$\hat{U}_2 = \exp\left(\frac{2\pi i}{L_x L_y} \sum_{x=1}^{L_x} \sum_{y=1}^{L_y} xy \hat{n}_{(x,y)}\right), \quad (\text{E4})$$

where $\hat{n}_{(x,y)}$ is the occupation number operator at site (x, y) and we label the x - (y -)position of site (x, y) as $x = 1, 2, \dots, L_x$ ($y = 1, 2, \dots, L_y$).

First of all, at least within the finite-size calculation up to $L \sim 20$ and within the toy model, we found that, unlike $|\langle \hat{U}_1 \rangle|$, $|\langle \hat{U}_2 \rangle|$ seems to exhibit the exponential decay in $L = L_x = L_y$ as shown in FIG. 7 (b), even for the insulating ground state (here the Wannier sector is also gapped):

$$|\langle \hat{U}_2 \rangle| \sim e^{-\alpha L}, \quad (\text{E5})$$

where $\alpha > 0$ is an exponent characterizing the exponential decay. However, to conclude that this scaling behavior is generic for any insulator, we need more detailed and thorough calculations on various models. Keeping this in mind, at this moment we would like to modestly mention that the scaling behaviors of the modulus of $\langle \hat{U}_2 \rangle$ is quite different from those of \hat{U}_1 . Despite of exponentially vanishing modulus for the models that we consider, the complex phases of the expectation value can be reliably measured for the typical system sizes that we worked on, e.g., $L \sim 10 - 20$. We also have checked that the Dirac semimetal state, which has a zero energy gap, also shows an exponential decay (with different exponent) in system size L .

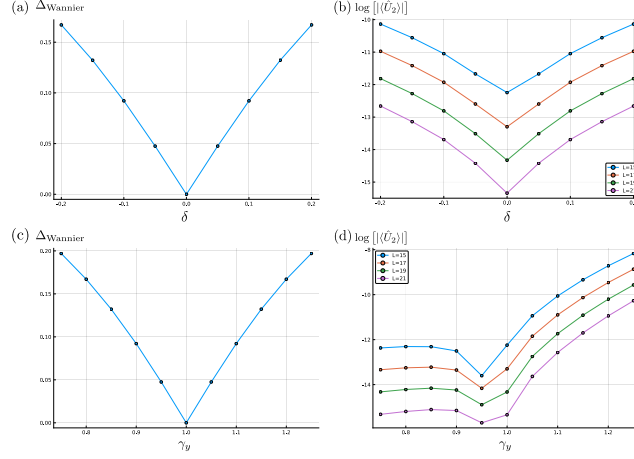


FIG. 8. Comparison between the Wannier gap and the modulus of $|\langle \hat{U}_2 \rangle|$ for topological quadrupole insulator Eq. (D4). In (a) and (b) we fix $(\gamma_x, \gamma_y, \lambda_y, \lambda_x, \lambda_y) = (0.75, 1.0, 1.0, 1.0)$ and tune $\delta \in [-0.2, 0.2]$. When $\delta = 0$ (a) the Wannier gap closes and (b) $|\langle \hat{U}_2 \rangle|$ is the smallest. In (c) and (d) we fix $(\gamma_x, \lambda_x, \lambda_y, \delta) = (0.75, 1.0, 1.0, 0.0)$ and tune $\gamma_y \in [0.75, 1.25]$. (c) The Wannier gap associated with the Wannier band $\nu_x(k_y)$ closes at $\gamma_y = 1.0$ and (d) $|\langle \hat{U}_2 \rangle|$ is the smallest around $\gamma_y = 1.0$. In all cases, the Wannier gap is well-defined in the thermodynamic limit while $|\langle \hat{U}_2 \rangle|$ vanishes exponentially in system size L .

Second, we perform the comparative studies of the modulus with the Wannier gap. For this we use the model of the topological quadrupole insulator Eq. (D5) with $\delta = 0$. Here the topological-to-trivial quadrupole insulator transition is associated with the Wannier gap closing transition while the bulk gap may not close at the transition point⁷. To see how $\langle \hat{U}_2 \rangle$ detects such quantum phase transition, we compute $|\langle \hat{U}_2 \rangle|$ across the phase transition. Due to the quantization by symmetries, $\langle \hat{U}_2 \rangle$ is a real number and changes its sign across the phase transition. So precisely at the transition point, $\langle \hat{U}_2 \rangle$ vanishes up to the correction from finite-size effect. In FIG. 8, we present two scenarios of Wannier-gap closing transition, one by tuning δ and the other by tuning λ_y . We see that whenever the Wannier gap closes, $|\langle \hat{U}_2 \rangle|$ also becomes the smallest.

2. Dependence on Coordinate Parameterization

As outlined in the main text, our many-body operators as well as the original Resta's operator can be generalized by acting only on subsystem and/or change in the boundary conditions. In this subsection, we would like to discuss the dependence on the coordinate parametrization on the many-body operators. To be precise, let us consider the following many-body operator which takes into account both the partial action and the coordinate parametrization issue.

$$\hat{V}_1(l, d) = \begin{cases} \exp \left[\frac{2\pi i}{l} \sum_x (x-d)(\hat{n}_x - \bar{n}) \right] & \text{for } x \in [1, l] \\ 1 & \text{otherwise} \end{cases}, \quad (\text{E6})$$

where we consider a finite system with size L , $l > 0$ is an integer smaller than or equal to L , atomic sites are labeled by $x \in \{1, 2, \dots, L\}$, and \bar{n} is the average filling per site. Similarly for quadrupole moment,

$$\hat{V}_2(l, d) = \begin{cases} \exp \left[\frac{2\pi i}{l^2} \sum_{\mathbf{r}=(x,y)} (x-d)(y-d)(\hat{n}_{\mathbf{r}} - \bar{n}) \right] & \text{for } \mathbf{r} \in [1, l] \times [1, l] \\ 1 & \text{otherwise} \end{cases}, \quad (\text{E7})$$

where the total system size is given by (L, L) , $l > 0$ is an integer less than or equal to L , sites are labeled by $x, y \in \{1, 2, \dots, L\}$, and \bar{n} denotes the average filling per site. Here, we present the isotropic case, but anisotropic as well as generalization to higher-order moments is immediate. Note that these are almost the same as the formula Eq. (6) and Eq. (7) in the main text, but with an extra phase factors $\sim \exp(2\pi i \bar{n})$. Here d parametrizes the dependence on the ‘‘origin’’ of the coordinate systems.

Now we present numerical evaluation of $\hat{V}_1(l, d)$ Eq. (E6) and $\hat{V}_2(l, d)$ Eq. (E7) in the case of SSH chain Eq. (D3) and topological quadrupole insulator Eq. (D5). Here, l denotes the linear system size within which the operator

$V_n(l, d)$ acts nontrivially and d tunes the choice of the origin of our system. In FIG. 9, we present the results for $\delta = 0$ and $\delta = 0.1$, where the former has the quantization symmetries and the latter does not. We set $(\gamma, \lambda) = (1.0, 2.0)$ for FIG. 9 (a) and (c), and set $(\gamma_x, \gamma_y, \lambda_x, \lambda_y) = (1.0, 1.0, 2.0, 2.0)$ for FIG. 9 (b) and (d). Hence for FIG. 9 (a) (FIG. 9 (b)), the ground state has topologically nontrivial polarization (quadrupole moment).

As expected, when $l = L$, $\langle \hat{V}_1(l = L, d) \rangle$, which is the original Resta's operator, is independent of d due to the charge conservation in the ground state. However, this is no longer true for $\langle \hat{V}_1(l < L, d) \rangle$ and $\langle \hat{V}_2(l, d) \rangle$ for all l , which is summarized in FIG. 9 (a) and (b). As a result, for some choices of l and d , the complex phase of $\langle \hat{V}_n(l, d) \rangle$ fails in capturing the ground state topological multipole moments. When $\delta = 0.1$, quantization of $\langle \hat{V}_n(l, d) \rangle$ no longer exists and its complex phase can take arbitrary value, which can be seen in FIG. 9 (c) and (d).

This behavior can be easily explained by considering the ultra-short correlated states. For the illustrational purpose, we take the topological and trivial ground states of the polarization chain.

$$|GS_{\text{triv}}\rangle = \prod_{n \in \mathbb{Z}} |n\rangle, \quad |GS_{\text{top}}\rangle = \prod_{n \in \mathbb{Z}} |n + \frac{1}{2}\rangle. \quad (\text{E8})$$

For these ground states, we see that $\langle GS_{\text{triv}} | \hat{V}_1(l, \frac{l}{2}) | GS_{\text{triv}} \rangle = \langle GS_{\text{top}} | \hat{V}_1(l, \frac{l}{2}) | GS_{\text{top}} \rangle = 1$, signaling that the two states cannot be distinguished if $d = \frac{l}{2}$. Similar discussion can be made for the quadrupole insulators, too, and this explains the lumps appearing in the numerical data Fig. 9.

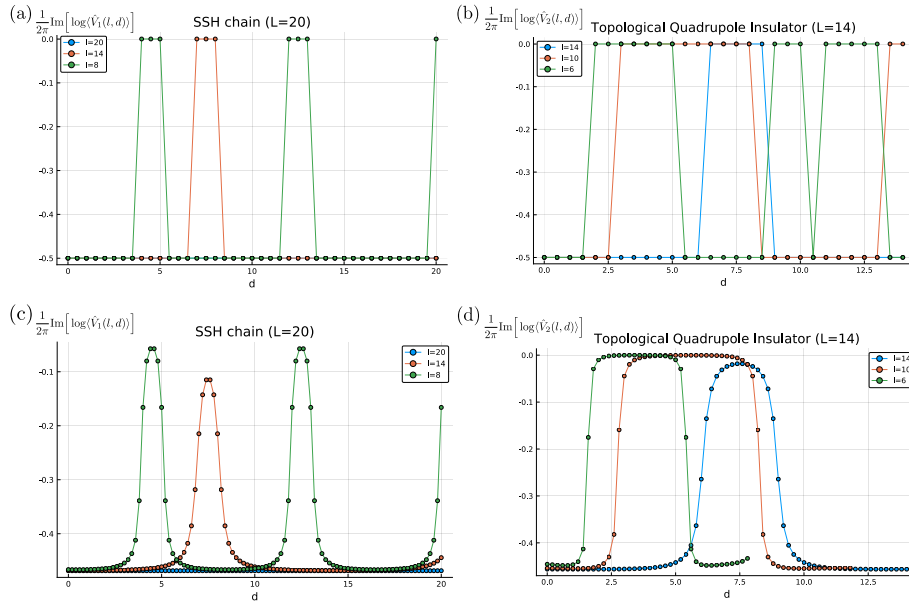


FIG. 9. The complex phase of $\langle \hat{V}_1(l, d) \rangle$ and $\langle \hat{V}_2(l, d) \rangle$ for various l 's as a function of d . (a) and (c) correspond to the SSH chain Eq. (D3) where we set $(\gamma, \lambda) = (1.0, 2.0)$ and (c) $\delta = 0$ and (d) $\delta = 0.1$. (b) and (d) correspond to the topological quadrupole insulator Eq. (D5) where we set $(\gamma_x, \gamma_y, \lambda_x, \lambda_y) = (1.0, 1.0, 2.0, 2.0)$ and (c) $\delta = 0$ and (d) $\delta = 0.1$. While the ground state of (a) and (b) are topologically nontrivial, for some l and d the complex phase of $\langle \hat{V}_n(l, d) \rangle$ becomes trivial. In (c) and (d), as a function of d we see “lumps”.

-
- ¹ H. Watanabe and M. Oshikawa, Phys. Rev. X **8**, 021065 (2018).
 - ² W. A. Benalcazar, B. A. Bernevig, and T. L. Hughes, Science **357**, 61 (2017).
 - ³ H. Song, S.-J. Huang, L. Fu, and M. Hermele, Phys. Rev. X **7**, 011020 (2017).
 - ⁴ K. Shiozaki, C. Z. Xiong, and K. Gomi, arXiv preprint arXiv:1810.00801 (2018).
 - ⁵ Z. Song, C. Fang, and Y. Qi, arXiv preprint arXiv:1810.11013 (2018).
 - ⁶ K. Shiozaki, H. Shapourian, and S. Ryu, Phys. Rev. B **95**, 205139 (2017).
 - ⁷ W. A. Benalcazar, B. A. Bernevig, and T. L. Hughes, Phys. Rev. B **96**, 245115 (2017).
 - ⁸ G. Y. Cho, C.-T. Hsieh, T. Morimoto, and S. Ryu, Phys. Rev. B **91**, 195142 (2015).

- ⁹ H. Shapourian, K. Shiozaki, and S. Ryu, Phys. Rev. Lett. **118**, 216402 (2017).
- ¹⁰ W. P. Su, J. R. Schrieffer, and A. J. Heeger, Phys. Rev. Lett. **42**, 1698 (1979).
- ¹¹ S. Franca, J. van den Brink, and I. C. Fulga, Phys. Rev. B **98**, 201114 (2018).
- ¹² R. Resta, Phys. Rev. Lett. **80**, 1800 (1998).
- ¹³ J. Zak, Phys. Rev. Lett. **62**, 2747 (1989).
- ¹⁴ R. Resta and S. Sorella, Phys. Rev. Lett. **82**, 370 (1999).
- ¹⁵ R. Kobayashi, Y. O. Nakagawa, Y. Fukusumi, and M. Oshikawa, Phys. Rev. B **97**, 165133 (2018).